THIS DOCUMENT PROVIDED BY THE ABBOTT AEROSPACE
TECHNICAL LIBRARY
ABBOTTAEROSPACE.COM

NASA TECHNICAL NOTE

NASA TN D-6777

NASA TN D-6777

FLIGHT-DETERMINED DERIVATIVES AND DYNAMIC CHARACTERISTICS OF THE CV-990 AIRPLANE

by Glenn B. Gilyard

Flight Research Center
Edwards, Calif. 93523

NATIONAL AERONAUTICS AND SPACE ADMINISTRATION • WASHINGTON, D. C. • MAY 1972

THIS DOCUMENT PROVIDED BY THE ABBOTT AEROSPACE
TECHNICAL LIBRARY
ABBOTTAEROSPACE.COM

1. Report No.	2. Government Accession No.	3. Recipient's Catalog No.
TN D-6777		

4. Title and Subtitle	5. Report Date
FLIGHT-DETERMINED DERIVATIVES AND DYNAMIC CHARACTERISTICS OF THE CV-990 AIRPLANE	May 1972
	6. Performing Organization Code
7. Author(s)	8. Performing Organization Report No.
Glenn B. Gilyard	H-693
	10. Work Unit No.
	126-62-10-00-24
9. Performing Organization Name and Address	11. Contract or Grant No.
NASA Flight Research Center P. O. Box 273 Edwards, California 93523	
	13. Type of Report and Period Covered
12. Sponsoring Agency Name and Address	Technical Note
National Aeronautics and Space Administration Washington, D. C. 20546	14. Sponsoring Agency Code

15. Supplementary Notes

16. Abstract

Flight-determined longitudinal and lateral-directional stability and control derivatives are presented for the CV-990 airplane for various combinations of Mach number, altitude, and flap setting throughout the flight envelope up to a Mach number of 0.87. Also presented are the dynamic characteristics of the aircraft calculated from the flight-obtained derivatives and the measured phugoid characteristics. The derivative characteristics were obtained from flight records of longitudinal and lateral-directional transient oscillation maneuvers by using a modified Newton-Raphson digital derivative determination technique.

Generally the derivatives exhibited consistent variation with lift coefficient in the low-speed data and with Mach number and altitude in the high-speed data. Many also varied with flap deflection, notably spoiler effectiveness and directional stability.

17. Key Words (Suggested by Author(s))	18. Distribution Statement
Subsonic transport Flight-determined derivatives Dynamic characteristics	Unclassified - Unlimited

19. Security Classif. (of this report)	20. Security Classif. (of this page)	21. No. of Pages	22. Price*
Unclassified	Unclassified	65	$3.00

*For sale by the National Technical Information Service, Springfield, Virginia 22151

THIS DOCUMENT PROVIDED BY THE ABBOTT AEROSPACE
TECHNICAL LIBRARY
ABBOTTAEROSPACE.COM

FLIGHT-DETERMINED DERIVATIVES AND DYNAMIC CHARACTERISTICS OF THE CV-990 AIRPLANE

Glenn B. Gilyard
Flight Research Center

INTRODUCTION

Although jet transports have been in operation about 10 years, there is little published information on the basic aerodynamic characteristics of this class of aircraft. Documentation of the stability and control derivatives and characteristics of a representative aircraft of this class would provide useful baseline data for comparison with design trends of future transports and for use in simulation studies. To provide such documentation, a flight program was conducted on a NASA-operated CV-990 transport which included investigations of stalls (ref. 1), landings, ground effects, noise (ref. 2), handling qualities (refs. 3 and 4), and aerodynamic characteristics.

This report documents a wide range of aerodynamic stability and control derivatives obtained from stability and control maneuvers by using a newly developed digital-computer matching program (Newton-Raphson method described in ref. 5). The report also includes the calculated longitudinal short-period and Dutch roll characteristics of the airplane as well as measured phugoid characteristics.

The longitudinal and lateral-directional derivatives are presented for flight conditions from 120 knots to 195 knots indicated airspeed at an altitude of approximately 3960 meters (13,000 feet) with the airplane in various landing configurations and for Mach numbers from 0.40 to 0.87 at altitudes of 6096 meters and 10,670 meters (20,000 feet and 35,000 feet) in the cruise configuration.

SYMBOLS

Physical quantities in this report are given in the International System of Units (SI) and parenthetically in U.S. Customary Units. The measurements were taken in Customary Units. Factors relating the two systems are presented in reference 6.

a_n	normal acceleration at center of gravity, g units
a_t	transverse acceleration at center of gravity, g units
b	wing span, meters (feet)

THIS DOCUMENT PROVIDED BY THE ABBOTT AEROSPACE
TECHNICAL LIBRARY
ABBOTTAEROSPACE.COM

C_L lift coefficient, $\frac{\text{Lift}}{\bar{q}S}$

C_l rolling-moment coefficient, $\frac{\text{Rolling moment}}{\bar{q}Sb}$

$C_{l_p} = \frac{\partial C_l}{\partial \frac{pb}{2V}}$, per radian

$C_{l_r} = \frac{\partial C_l}{\partial \frac{rb}{2V}}$, per radian

$C_{l_\beta} = \frac{\partial C_l}{\partial \beta}$, per radian

$C_{l_{\delta_a}} = \frac{\partial C_l}{\partial \delta_a}$, per radian

$C_{l_{\delta_r}} = \frac{\partial C_l}{\partial \delta_r}$, per radian

$C_{l_{\delta_s}} = \frac{\partial C_l}{\partial \delta_s}$, per radian

C_m pitching-moment coefficient, $\frac{\text{Pitching moment}}{\bar{q}S\bar{c}}$

$C_{m_q} = \frac{\partial C_m}{\partial \frac{q\bar{c}}{2V}}$, per radian

$C_{m_\alpha} = \frac{\partial C_m}{\partial \alpha}$, per radian

$C_{m_{\delta_e}} = \frac{\partial C_m}{\partial \delta_e}$, per radian

C_N normal-force coefficient, $\frac{\text{Normal force}}{\bar{q}S}$

$C_{N_q} = \frac{\partial C_N}{\partial \frac{q\bar{c}}{2V}}$, per radian

THIS DOCUMENT PROVIDED BY THE ABBOTT AEROSPACE
TECHNICAL LIBRARY
ABBOTTAEROSPACE.COM

$C_{N_\alpha} = \frac{\partial C_N}{\partial \alpha}$, per radian

$C_{N_{\delta_e}} = \frac{\partial C_N}{\partial \delta_e}$, per radian

C_n yawing-moment coefficient, $\frac{\text{Yawing moment}}{\bar{q}Sb}$

$C_{n_p} = \frac{\partial C_n}{\partial \frac{pb}{2V}}$, per radian

$C_{n_r} = \frac{\partial C_n}{\partial \frac{rb}{2V}}$, per radian

$C_{n_\beta} = \frac{\partial C_n}{\partial \beta}$, per radian

$C_{n_{\delta_a}} = \frac{\partial C_n}{\partial \delta_a}$, per radian

$C_{n_{\delta_r}} = \frac{\partial C_n}{\partial \delta_r}$, per radian

$C_{n_{\delta_s}} = \frac{\partial C_n}{\partial \delta_s}$, per radian

C_Y lateral-force coefficient, $\frac{\text{Lateral force}}{\bar{q}S}$

$C_{Y_p} = \frac{\partial C_Y}{\partial \frac{pb}{2V}}$, per radian

$C_{Y_r} = \frac{\partial C_Y}{\partial \frac{rb}{2V}}$, per radian

$C_{Y_\beta} = \frac{\partial C_Y}{\partial \beta}$, per radian

$C_{Y_{\delta_a}} = \frac{\partial C_Y}{\partial \delta_a}$, per radian

THIS DOCUMENT PROVIDED BY THE ABBOTT AEROSPACE
TECHNICAL LIBRARY
ABBOTTAEROSPACE.COM

$C_{Y_{\delta_r}} = \frac{\partial C_Y}{\partial \delta_r}$, per radian

$C_{Y_{\delta_s}} = \frac{\partial C_Y}{\partial \delta_s}$, per radian

$\bar{c}$ mean aerodynamic chord, meters (feet)

g acceleration due to gravity, meters/second^2 (feet/second^2)

h_p pressure altitude, meters (feet)

I_X, I_Y, I_Z moments of inertia about X-, Y-, and Z-body axes, respectively, kilogram-meter^2 (slug-foot^2)

I_{XZ} product of inertia referred to the body X- and Z-axes, kilogram-meter^2 (slug-foot^2)

$L_p = C_{l_p} \frac{\bar{q}Sb^2}{2VI_X}$, 1/second

$L_r = C_{l_r} \frac{\bar{q}Sb^2}{2VI_X}$, 1/second

$L_\beta = C_{l_\beta} \frac{\bar{q}Sb}{I_X}$, 1/second^2

$L_{\delta_a} = C_{l_{\delta_a}} \frac{\bar{q}Sb}{I_X}$, 1/second^2

$L_{\delta_r} = C_{l_{\delta_r}} \frac{\bar{q}Sb}{I_X}$, 1/second^2

$L_{\delta_s} = C_{l_{\delta_s}} \frac{\bar{q}Sb}{I_X}$, 1/second^2

l distance from center of gravity to center of pressure of the elevator, meters (feet)

M Mach number

$M_q = C_{m_q} \frac{\bar{q}S\bar{c}^2}{2VI_Y}$, 1/second

$M_\alpha = C_{m_\alpha} \frac{\bar{q}S\bar{c}}{I_Y}$, 1/second^2

THIS DOCUMENT PROVIDED BY THE ABBOTT AEROSPACE
TECHNICAL LIBRARY
ABBOTTAEROSPACE.COM

$M_{\delta_e} = C_{m_{\delta_e}} \frac{\bar{q}S\bar{c}}{I_Y}$, $1/\text{second}^2$

m airplane mass, kilograms (slugs)

$N_p = C_{n_p} \frac{\bar{q}Sb^2}{2VI_Z}$, $1/\text{second}$

$N_q = C_{N_q} \frac{\bar{q}S\bar{c}}{2mV^2}$

$N_r = C_{n_r} \frac{\bar{q}Sb^2}{2VI_Z}$, $1/\text{second}$

$N_\alpha = C_{N_\alpha} \frac{\bar{q}S}{mV}$, $1/\text{second}$

$N_\beta = C_{n_\beta} \frac{\bar{q}Sb}{I_Z}$, $1/\text{second}^2$

$N_{\delta_a} = C_{n_{\delta_a}} \frac{\bar{q}Sb}{I_Z}$, $1/\text{second}^2$

$N_{\delta_e} = C_{N_{\delta_e}} \frac{\bar{q}S}{mV}$, $1/\text{second}$

$N_{\delta_r} = C_{n_{\delta_r}} \frac{\bar{q}Sb}{I_Z}$, $1/\text{second}^2$

$N_{\delta_s} = C_{n_{\delta_s}} \frac{\bar{q}Sb}{I_Z}$, $1/\text{second}^2$

P	period, seconds
p, q, r	roll, pitch, and yaw rate, respectively, radians/second (unless otherwise noted)
$\dot{p}, \dot{q}, \dot{r}$	roll, pitch, and yaw acceleration, respectively, radians/second^2
$\bar{q}$	dynamic pressure, newtons/meter^2 (pounds/foot^2)
S	wing area, meters^2 (feet^2)
τ_r	roll mode time constant, seconds
τ_s	spiral mode time constant, seconds

THIS DOCUMENT PROVIDED BY THE ABBOTT AEROSPACE
TECHNICAL LIBRARY
ABBOTTAEROSPACE.COM

$T_{1/2}$ — time for transient oscillation to damp to half amplitude, seconds

t — time, seconds

V — velocity, meters/second (feet/second)

W — airplane weight, kilograms (pounds)

x_α, x_β — distance from center of gravity to angle-of-attack and angle-of-sideslip sensors, respectively, positive forward, meters (feet)

$$Y_p = C_{Y_p} \frac{\bar{q}Sb}{2mV^2}$$

$$Y_r = C_{Y_r} \frac{\bar{q}Sb}{2mV^2}$$

$$Y_\beta = C_{Y_\beta} \frac{\bar{q}S}{mV}, \text{ 1/second}$$

$$Y_{\delta_a} = C_{Y_{\delta_a}} \frac{\bar{q}S}{mV}, \text{ 1/second}$$

$$Y_{\delta_r} = C_{Y_{\delta_r}} \frac{\bar{q}S}{mV}, \text{ 1/second}$$

$$Y_{\delta_s} = C_{Y_{\delta_s}} \frac{\bar{q}S}{mV}, \text{ 1/second}$$

α — angle of attack at center of gravity, radians (unless otherwise noted)

α_i — instrument indicated angle of attack, degrees

β — angle of sideslip at center of gravity, radians (unless otherwise noted)

β_i — instrument indicated angle of sideslip, degrees

$\dot{\alpha}, \dot{\beta}$ — α and β rates, radians/second

Δ — incremental change

THIS DOCUMENT PROVIDED BY THE ABBOTT AEROSPACE
TECHNICAL LIBRARY
ABBOTTAEROSPACE.COM

$\delta_a, \delta_r, \delta_s, \delta_e, \delta_f$	average aileron, rudder, spoiler, elevator, and Fowler flap deflection, respectively; positive: trailing edge of rudder left, aileron and spoiler deflections which produce right roll, elevator trailing edge down, Fowler flap trailing edge down; radians (unless otherwise noted)
δ_w	wheel displacement, positive clockwise, degrees
ϵ	angle between body X-axis and principal X-axis, positive when body axis is below principal axis at nose of airplane
ζ	damping ratio
θ, φ	Euler angle of pitch and roll, respectively, radians (unless otherwise noted)
$\dot{\theta}, \dot{\varphi}$	θ and φ rates, radians/second (unless otherwise noted)

Subscripts:

i	indicated
o	initial

AIRPLANE DESCRIPTION

The CV-990 airplane (figs. 1 and 2 and table 1) is representative of the low-wing jet transports now in operation. It has a design cruise Mach number of approximately 0.85 between 10,670 meters and 12,192 meters (35,000 feet and 40,000 feet) altitude. The wing and tail are both swept 35° at the 30-percent-chord line. The dihedral of the wing is 7°; the dihedral of the tail is 7.5°. The basic commercial version has a dry weight of 67,132 kilograms (148,000 pounds) and a design gross takeoff weight of 111,585 kilograms (246,000 pounds). The version tested was unfurnished and had a dry weight of 56,700 kilograms (125,000 pounds) and, with maximum fuel, a gross takeoff weight of 101,152 kilograms (223,000 pounds). Normal flap deflections are 27° for takeoff and 50° for approach and landing.

The airplane has two antishock bodies on each wing that are used to store fuel and to reduce transonic drag rise. The propulsion is provided by four General Electric CJ805-23 aft-fan turbojets which are pod-mounted and suspended below and forward of the wing on highly swept pylons.

Longitudinal Controls

The primary longitudinal control is the elevator, which is operated by the aerodynamic forces of the mechanically operated elevator flight tabs. The limits of the elevator are 25° up and 12° down; the flight tab limits are 12° up and 25° down with respect to the elevator. The control column forces are minimized by the aerodynamic

THIS DOCUMENT PROVIDED BY THE ABBOTT AEROSPACE
TECHNICAL LIBRARY
ABBOTTAEROSPACE.COM

balance of the tabs.

A completely movable horizontal stabilizer provides the gross longitudinal trim required on takeoffs and landings and the Mach trim required in the tuck region.[1] The limits of the horizontal stabilizer are 2.5° leading edge up and 13.25° leading edge down.

Slotted (Fowler) flaps are incorporated in the trailing-edge section of each wing, on either side of the ailerons. The flaps are hydraulically actuated and have five detent positions corresponding to 0°, 10°, 27°, 36°, and 50° (full down). There are eight leading-edge (Krueger) flaps on each wing. Each flap has two positions (fully retracted and fully extended), is hydraulically actuated, and is controlled by the trailing-edge-flap lever according to the following schedule:

Trailing-edge (Fowler) flaps	Leading-edge (Krueger) flaps
0°	All retracted
10° and 27°	All extended
36° and 50°	All extended, except inboard flap

Lateral Controls

The ailerons are positioned by aileron tabs and operated from the pilot's wheel. The maximum deflection of the pilot's wheel mechanically commands the maximum aileron flight tab travel of ±20° which, through the aerodynamic boost, operates the ailerons with a maximum travel of ±15°.

The spoilers, which provide approximately 80 percent of the roll control power, are directly connected to the copilot's wheel. The maximum spoiler deflection is 75° for the inboard spoilers and 60° for the outboard spoilers for indicated airspeeds of less than 200 knots. For airspeeds greater than 200 knots, the spoilers have a blow-down feature, because the actuators do not have enough power to command full deflection. The outboard spoilers can reach the maximum deflection in 1 second, whereas the inboard spoilers require 1.25 seconds. The spoilers can be disconnected from the lateral control system to permit aileron-only control. The pilot's and copilot's controls are interconnected in the cockpit. The variation of aileron and spoiler deflection is presented in figure 3 for the normal range of wheel usage.

Directional Controls

In normal operation, the rudder is hydraulically actuated and has a total travel of ±25°. The rudder flight tab is deflected with the rudder in a 1 to 1 ratio, thus providing additional control power. The rudder also receives commands from a yaw damper computer proportional to yaw rate, r, and yaw acceleration, $\dot{r}$. These commands are obtained by taking the difference of two longitudinally displaced lateral accelerometers to produce the $\dot{r}$ term and then introducing lag in the $\dot{r}$ loop to yield the r component.

[1] Transonic region where airplane has a natural tendency to nose down.

THIS DOCUMENT PROVIDED BY THE ABBOTT AEROSPACE
TECHNICAL LIBRARY
ABBOTTAEROSPACE.COM

INSTRUMENTATION

The recording instrumentation used is listed in table 2. Angular accelerometers were not used. The instrumentation was alined with the body axes, and the angle-of-attack and angle-of-sideslip vanes were mounted on a nose boom which also contained an airspeed-altitude probe.

The data were recorded by three 15.24-centimeter- (6-inch-) throw, 26-channel oscillographs. The data were read at 0.1-second intervals, with the length of the runs varying from 10 seconds for heavily damped short-period longitudinal data to 25 seconds for lightly damped Dutch roll data.

Table 2 lists the ranges of the various sensors and the total cumulative errors estimated from the following sources: transducer, recording system, zeros, and calibration. The error introduced by the reader was nil. Because of zero-shift errors in the recording system, the angle-of-attack values in table 3 were taken mainly from pilot notes.

TEST CONDITIONS

The Mach number and altitude conditions at which data were obtained are shown in figure 4; pertinent aircraft conditions are given in table 3. All the data were obtained at preselected Mach and altitude conditions, but at existing weights and center-of-gravity positions. Although the gross weight and center of gravity were measured, corresponding moments of inertia were estimated (table 3) on the basis of limited data from the manufacturer. Because of the uncertainty of the inertias, the derivatives are presented in dimensional as well as nondimensional form.

Pullup and release maneuvers were used to determine the longitudinal derivatives. The phugoid mode was also excited to measure phugoid characteristics. The lateral-directional set of maneuvers consisted of a rudder doublet, aileron-plus-spoiler doublet, and an aileron-only doublet. All the maneuvers were started from a level trim condition at a selected altitude with the Mach trim and yaw damper off except for four maneuvers made with the yaw damper on.

DATA AND ACCURACY ANALYSIS

Data Analysis

The longitudinal short-period damping ratio was high enough (0.4 to 0.8) to make simple methods of analysis impracticable. However, the lateral-directional maneuvers were lightly damped ($\zeta < 0.075$) so that control-fixed free oscillations could be analyzed by using the time vector method (ref. 7). The vector method results were used primarily to check the derivatives obtained with the more versatile, newly developed, Newton-Raphson derivative extraction technique used throughout the analysis (ref. 5). The equations used in the analysis are presented in appendix A, and the application of the Newton-Raphson technique during this investigation is discussed in appendix B.

THIS DOCUMENT PROVIDED BY THE ABBOTT AEROSPACE
TECHNICAL LIBRARY
ABBOTTAEROSPACE.COM

The basic principle of the Newton-Raphson technique is that deviations between flight and calculated time histories of airplane response to control inputs are minimized. The calculated time histories were based on the mathematical model described in appendix A. Typical matches, which represent the landing and cruise configurations, are presented in figures 5 and 6 for the longitudinal short-period mode and Dutch roll mode, respectively.

The frequency, damping, and dynamic characteristics were calculated from the final set of flight derivatives.

Although only one longitudinal maneuver for each flight condition was considered necessary for analysis purposes, three lateral-directional maneuvers were required to provide sufficient dynamic data to obtain consistent results. The need for several lateral-directional maneuvers first became evident when separate matches of several available maneuvers, for any one flight condition, did not yield a unique set of derivatives. That is to say, some of the derivatives obtained from matching independently a rudder doublet, an aileron doublet, and an aileron-plus-spoiler doublet were significantly different. However, by matching all the lateral-directional doublet maneuvers simultaneously at a specific flight condition, a unique set of derivatives was apparently obtained.

Although the ailerons and spoilers did not move together in a precise ratio, the phasing of their motions was so nearly identical that the effectiveness of each surface could not be determined individually by the Newton-Raphson method. The aileron-only doublet, however, provided the additional information required to simultaneously separate the two control derivatives. The aileron control derivatives are determined primarily from the information content of the aileron-only maneuvers and the spoiler derivatives are determined from the information contained in the aileron-plus-spoiler maneuvers. In all instances the consistency of the derivatives increased with the number of maneuvers being matched simultaneously.

Early in the program, aileron-only doublet data were not obtained, hence a yaw-damper-on doublet was also matched with the rudder and aileron-plus-spoiler doublets for improved accuracy.

A data sample rate of 10 points per second was used to match the time histories of the longitudinal mode, whereas a 5-point-per-second rate was used for the lateral-directional mode. Because the aircraft inertias were not accurately known, the cross product of inertia was assumed to be zero. Available data from the manufacturer also indicated that this assumption was valid. Further information on assumed inertias and data sample rate is presented in appendix B.

Accuracy Analysis

With the Newton-Raphson method an indication of the quality or the confidence level of each derivative is computed in terms of a variance. The variance is determined with respect to every other derivative and variable of a particular match and is defined as the lower bound of the standard deviation, provided certain assumptions about the data are valid. The basic assumption is that the data being analyzed can be accurately described by the model with only white noise superimposed. Reference 5 shows that although this basic assumption is not exactly met, for engineering purposes it is

THIS DOCUMENT PROVIDED BY THE ABBOTT AEROSPACE
TECHNICAL LIBRARY
ABBOTTAEROSPACE.COM

satisfied. The use of the variance, however, is of limited value because the definition implies that if the variance is small, the derivative could (although need not necessarily) be well defined, whereas if the variance is large, it can be assumed that the derivative is poorly defined.

Table 4 shows the average variance of each derivative and the probable-error index, which is defined as the average ratio of the variance to the derivative magnitude in percent. As would be expected, the static stability derivatives and the major control derivatives have a low probable-error index, which indicates that the quality of these derivatives is good. The probable-error index is not meaningful and therefore not presented for derivatives having values approaching or passing through zero, or both.

RESULTS AND DISCUSSION

In the following analysis, the airplane stability and control derivatives are related to such variables as lift coefficient, Mach number, and flap setting. Initially, angle of attack was chosen because classically it is the most used parameter. However, the zero corrections for the angle-of-attack indicator varied from flight to flight and on a few flights were not obtained. As a result, the angle-of-attack measurements were not completely reliable. The derivatives are therefore related to lift coefficient, a more accurate parameter which is dependent only on airplane weight, normal acceleration, and dynamic pressure.

Longitudinal Stability and Control Derivatives

The longitudinal derivatives obtained from the analysis of pullup and release maneuvers are presented in terms of lift coefficient for the low-speed flight conditions and in terms of Mach number for the clean configuration flight conditions. The pitching moment and normal-force derivatives are presented in figures 7 and 8, respectively.

Because the high-speed derivatives are plotted in terms of Mach number, the data at constant altitude contain angle-of-attack and dynamic-pressure effects which in turn affect aeroelasticity. Dynamic-pressure effects could not be isolated with the available flight data because of lack of control over the flight conditions. The dynamic characteristics calculated from the flight-obtained derivatives are presented in figure 9 together with measured phugoid characteristics. Dimensional body-axis derivatives are given in table 5.

Stability derivatives.– In order to provide meaningful comparisons, the static stability derivative, C_{m_α}, was corrected to $0.25\bar{c}$. Figure 7 shows C_{m_α} to be nearly invarient with C_L for the low-speed conditions with the flaps set at 50°; however, the data do not appear to show a consistent trend with the flaps at 27°. On the other hand, the clean configuration data show a fairly consistent difference between the data for 6096 meters and 10,670 meters (20,000 feet and 35,000 feet) altitude. This indicates a significant effect of lift coefficient at any one Mach number and possibly also aeroelasticity with increasing Mach number as reflected in the relative trends of the constant C_L lines in the figure. Transonic effects could also be a factor at the

THIS DOCUMENT PROVIDED BY THE ABBOTT AEROSPACE
TECHNICAL LIBRARY
ABBOTTAEROSPACE.COM

higher Mach numbers.

The damping derivative, C_{m_q} (fig. 7), increases negatively with increasing C_L for low-speed flight conditions. The data indicate a slight decrease in C_{m_q} resulting from lowering the flaps from 27° to 50°. In general, the higher damping of the low-speed maneuvers gave rise to greater uncertainties in the data analysis. At high speeds C_{m_q} shows a definite increasing trend with increasing Mach number but does not vary significantly with C_L. The discrepancies at $C_L = 1.2$ for 50° flaps, and the one at $M = 0.80$, $h_p = 10,670$ meters (35,000 feet), are believed to be due to poorly conditioned maneuvers.

The lift-curve slope, C_{N_α} (fig. 8), appears to decrease with increasing C_L at the low-speed conditions but shows no clear trend due to flap deflection. The high-speed trends for C_{N_α} also show C_L or aeroelastic effects, or both, as evidenced by differences between the 6096-meter and 10,670-meter (20,000-foot and 35,000-foot) data at the same Mach number. Although C_{N_α} increases with Mach number at a constant altitude, this is attributed partially to angle-of-attack variation.

At low speeds C_{N_q} (fig. 8) increases rapidly (in the positive direction) with increasing C_L. The rather large values of C_{N_q} at high lift coefficients have as much effect on airplane frequency as the usually more dominant derivative, C_{m_α}. Large values of C_{N_q} also produce significant transient lift effects during certification stall maneuvers. This high sensitivity of normal acceleration to pitch rate resulting from high values of C_{N_q} is shown more clearly in the following approximation:

$$\Delta a_n \text{ (due to q)} = \frac{V_o}{g} N_q q$$

$$\frac{\Delta a_n}{q} = \frac{V_o}{g} N_q \approx 0.068 \text{ g/deg/sec}$$

Scatter in the data precludes identification of possible flap effects.

At high speeds C_{N_q} shows a decreasing trend with increasing Mach number and decreasing altitude, tending toward zero and negative values at the high Mach numbers.

Control derivatives.– The pitch control derivative, $C_{m_{\delta_e}}$ (fig. 7), shows little

THIS DOCUMENT PROVIDED BY THE ABBOTT AEROSPACE
TECHNICAL LIBRARY
ABBOTTAEROSPACE.COM

variation with either lift coefficient or flap deflection at low speeds, and is essentially invariant with Mach number. The derivative $C_{N_{\delta_e}}$ (fig. 8) was not an independent variable in the derivative matching process but was calculated from the expression:

$$C_{N_{\delta_e}} = -\frac{\bar{c}}{l} C_{m_{\delta_e}}$$

Thus, $C_{N_{\delta_e}}$ is also approximately a constant for all flight conditions.

The Newton-Raphson method provides a measure of the variance of the determined derivatives. The average variance and the probable-error index, which is the percentage of the variance to the actual magnitude of the derivative, are given in table 4. These probable-error indexes indicate that C_{m_α} is the most reliable of the longitudinal set followed in order of descending reliability by $C_{m_{\delta_e}}$, C_{N_α}, and C_{m_q}. Although no probable-error index is presented for C_{N_q}, comparison of the average variance with each individual flight value of N_q (table 5(a)) clearly shows that C_{N_q} is the most poorly defined of the group. The quality of the derivatives is generally consistent with results from other methods of analysis such as analog matching (ref. 7).

Short-Period Characteristics

The period and damping characteristics calculated from the flight-determined derivatives are presented in figure 9(a). The results appear to show consistent variation with Mach number and altitude despite the high damping (ζ = 0.4 to 0.8) of the maneuvers analyzed. The period, P, ranges from 15 seconds at the lowest speeds to 3 seconds at high speeds, and decreases with increasing Mach number (constant altitude) or decreasing altitude (constant Mach number) as a result of increasing dynamic pressure. Both ζ and $T_{1/2}$ show decreasing trends with increasing Mach number. None of the characteristics exhibits variation due to flap deflection.

Phugoid Characteristics

The phugoid period and damping characteristics measured from oscillograph records are presented in figure 9(b). Data are presented for the basic, unaugmented aircraft and for the aircraft with the Mach trim compensator engaged for Mach numbers greater than 0.50. Comparison of the phugoid period with the classical approximation, $P = \frac{\sqrt{2}\pi V}{g}$, shows the results for the low-speed, flaps-extended configurations to be consistently higher than predicted. Results for the clean configuration agree well with predictions at low Mach numbers, but fall substantially below predictions at high Mach numbers.

THIS DOCUMENT PROVIDED BY THE ABBOTT AEROSPACE
TECHNICAL LIBRARY
ABBOTTAEROSPACE.COM

The Mach trim compensator had no clear effect on the phugoid period below the tuck region. With the compensator disengaged, however, a tuck was observed at a Mach number of 0.87 and an altitude of 10,670 meters (35,000 feet). At other high-speed conditions ($M \geqq 0.85$) with the Mach trim compensator off, the airplane reached an overspeed condition within the first cycle of the phugoid oscillation.

The phugoid was divergent ($\zeta < 0$) at all Mach number and altitude conditions covered with the airplane in the clean configuration (fig. 9(b)), and the Mach trim compensator had no discernible effect on damping.

Deflection of the flaps revealed an interesting variation of phugoid damping with airspeed. The damping for flap settings of 27° and 50° steadily deteriorates as Mach number decreases to about 0.27 (140 knots) at which point the damping is essentially neutral for the 27° flap setting. Further reduction in speed is accompanied by a rapid increase in damping. This variation with speed is believed to result from a shift from the front side to the back side of the power curve as speed is reduced below about 140 knots. The point of minimum damping corresponds approximately to the point of maximum lift-to-drag ratio.

Lateral-Directional Derivatives

The derivatives and corresponding calculated dynamic characteristics for the lateral-directional modes are presented in figures 10 to 16. Included with the dynamic characteristics are data obtained with the yaw damper on. The dimensional body-axis derivatives are summarized in table 5.

Static stability derivatives.– The dihedral effect derivative, C_{l_β} (fig. 10), for the low-speed configurations shows a significant increasing trend with increasing lift coefficient and is essentially unchanged by flap deflection at any specific C_L. The data for the clean configuration show C_{l_β} increasing with altitude at constant Mach number, which indicates a pronounced increase with increasing C_L and thus increasing angle of attack. At constant altitude, C_{l_β} remains relatively constant with increasing Mach number and thus decreasing angle of attack, from which it may be inferred that an increase in C_{l_β} with increasing Mach number is counteracted by a decrease in C_{l_β} with decreasing angle of attack.

For the low-speed configurations the directional stability derivative, C_{n_β} (fig. 10), shows a significant decreasing trend with increasing lift coefficient at low speeds and a well-defined increase in directional stability with increasing flap deflection. Flap deflections from 0° to 27° and from 27° to 50° produce about equal incremental changes in C_{n_β}. The directional stability derivative shows an increase with Mach number at constant altitude caused primarily by angle-of-attack effects. The variation of C_{n_β} with altitude at a constant Mach number again reflects mainly angle-of-attack effects.

THIS DOCUMENT PROVIDED BY THE ABBOTT AEROSPACE
TECHNICAL LIBRARY
ABBOTTAEROSPACE.COM

There is no significant effect of lift coefficient on C_{Y_β} (fig. 10) for the C_L range investigated; however, within the scatter of the data there is a trend toward a slight increase (negatively) caused by lowering the flaps. For the clean configuration, C_{Y_β} appears to be unaffected by the variables considered.

On the basis of the probable-error indexes in table 4, it appears that C_{n_β}, C_{l_β}, and C_{Y_β} are the most accurate of the 16 derivatives determined.

Rotary derivatives.– The damping-in-roll derivative, C_{l_p} (fig. 11), was nearly constant for the low-speed configurations over the C_L range of these tests; however, increasing flap deflection does appear to result in a slight decrease in C_{l_p}. For the cruise configuration there does not appear to be a conclusive trend in the variation of C_{l_p} with Mach number and altitude; however, aerodynamic theory indicates a close relationship between C_{l_p} and C_{N_α}. A comparison of C_{l_p} (fig. 11) and C_{N_α} (fig. 8) suggests that the C_{l_p} value at a Mach number of 0.40 and the C_{l_p} value for an altitude of 10,670 meters (35,000 feet) at a Mach number of 0.70 are both high. If these possibilities are taken into account, C_{l_p} does increase with increasing Mach number. The probable-error index in table 4 shows that the damping-in-roll derivative was one of the more accurate derivatives determined.

The data for the directional damping derivative, C_{n_r} (fig. 11), for the configurations with flaps deflected indicate a decreasing trend with decreasing lift coefficient. There are no clearly discernible effects of flap position on the derivative. The results for the clean configuration show an average value of about -0.09, with no definite trend with Mach number. Table 4 shows that the probable-error index value for this derivative is among the highest and thus the accuracy or quality of the derivative is among the weakest.

In figure 12 the cross-coupled derivatives, C_{l_r} and C_{n_p}, although difficult to measure accurately, vary with lift coefficient in the low-speed configurations. The trends shown are typical inasmuch as the wing is the principal contributing element. There is a slight reduction in C_{n_p} with increasing flap deflection.

Data for the cruise configuration show considerable scatter in C_{l_r} and C_{n_p}, obscuring any trend with Mach number or angle of attack. The magnitudes of both C_{l_r} and C_{n_p} are near zero, so that only average variances could be presented meaningfully in table 4.

THIS DOCUMENT PROVIDED BY THE ABBOTT AEROSPACE
TECHNICAL LIBRARY
ABBOTTAEROSPACE.COM

The C_{Y_p} and C_{Y_r} derivatives were not determined because of their negligible effect on airplane response.

Control derivatives.– For the configurations with flaps deflected, figure 13 shows that the lateral spoiler effectiveness increases with lift coefficient and flap deflection, whereas the aileron effectiveness decreases with increasing lift coefficient and is not affected by flap deflection. The two derivatives are of approximately the same magnitude for the 27° flap configuration; however, it should be noted that most of the roll control was provided by the spoilers, which deflected approximately four times as much as the ailerons.

For the cruise configuration, the aileron and spoiler control derivatives show a definite Mach effect, which generally increases with increasing Mach number. There was no clear effect of lift coefficient on these derivatives.

The rudder cross-control derivative, $C_{l_{\delta_r}}$ (fig. 13), shows considerable variance with both C_L and Mach number but is clearly positive for all flight conditions investigated.

In figure 14 the rudder control power, $C_{n_{\delta_r}}$, in the low-speed configurations shows a clearly defined variation with lift coefficient, although little effect due to flap deflection is indicated. For the cruise configuration the rudder control effectiveness shows a steady decline with increasing Mach number at 6096 meters (20,000 feet). There is no conclusive trend with altitude or dynamic pressure.

The coefficient of yaw due to aileron control, $C_{n_{\delta_a}}$, was positive for all configurations and at all flight conditions studied (fig. 14). There is no apparent effect of lowering the flaps. In the clean configuration, $C_{n_{\delta_a}}$ shows an apparent Mach effect at an altitude of 10,670 meters (35,000 feet) but not at 6096 meters (20,000 feet).

The coefficient of yaw due to spoiler deflection, $C_{n_{\delta_s}}$ (fig. 14), for the configurations with flaps deflected is positive as expected and, like $C_{l_{\delta_s}}$, increased substantially as the flaps were lowered. Little, if any, effect of lift coefficient is indicated. For the cruise configuration, $C_{n_{\delta_s}}$ appears to be fairly constant with Mach number.

The side force control derivative, $C_{Y_{\delta_a}}$ (fig. 15), for the takeoff configuration shows a definable trend with C_L, changing from positive to negative values with increasing lift coefficient. Lowering the flaps to the landing configuration results in an apparent negative increase in this derivative. The derivative $C_{Y_{\delta_s}}$ (fig. 15) for the landing configuration exhibits an apparent variation with C_L, increasing from negative values at low C_L to positive values at high C_L. The derivative $C_{Y_{\delta_r}}$ shows

THIS DOCUMENT PROVIDED BY THE ABBOTT AEROSPACE
TECHNICAL LIBRARY
ABBOTTAEROSPACE.COM

an inconclusive variation with lift coefficient.

For the cruise configuration the side force control derivatives show no systematic trends with Mach number; however, $C_{Y_{\delta_r}}$ has a well-defined positive value whereas $C_{Y_{\delta_a}}$ and $C_{Y_{\delta_s}}$ are near zero.

The probable-error indexes for the roll and yaw control derivatives (table 4) are low except for $C_{l_{\delta_r}}$. The data for $C_{l_{\delta_r}}$ were generally of poor quality.

Lateral-Directional Dynamic Characteristics

The period and damping characteristics calculated from the flight-determined derivatives are presented as a function of Mach number in figure 16(a). Both P and $T_{1/2}$ decrease with increasing Mach number at constant altitude. A decrease is also noted with decreasing altitude at constant Mach number primarily as a result of dynamic-pressure effects. The damping ratio, ζ, on the other hand, increases with increasing Mach number and decreasing altitude to a maximum of 0.075. One maneuver, the aileron-only doublet at a Mach number of 0.70 and an altitude of 10,670 meters (35,000 feet), was near neutrally damped. This, in turn, was reflected as a noticeable increase in the time-to-damp-to-half amplitude and a reduction in ζ for this flight condition, as compared to the trends at other flight conditions. A comparison between the calculated period and damping characteristics and the values measured from the oscillograph records showed the differences to be negligible.

A few selected maneuvers made with the yaw damper on were analyzed. A comparison of the yaw-damper-on (fig. 16(b)) and yaw-damper-off data (fig. 16(a)) indicates a substantial increase in damping ratio attributable to the yaw damper.

Figure 16(c) presents the roll and inverse spiral mode time constants. The well-defined roll mode time constant, τ_r, is stable throughout the flight range for all configurations tested and decreases with increasing Mach number (constant altitude) and decreasing altitude (constant Mach number).

The results for the inverse spiral mode time constant, $\frac{1}{\tau_s}$, show considerable scatter, but the mode is evidently stable and thus agrees with pilot comments. The mode exhibits near-neutral stability with flaps deflected 50°. In general the time for the transient oscillation to damp to half amplitude, $T_{1/2}$, for the spiral mode is greater than 35 seconds.

CONCLUDING REMARKS

Longitudinal and lateral-directional stability and control derivatives determined from flight data by using the Newton-Raphson digital method are presented for various low-speed and cruise configurations of the CV-990 airplane. The airplane mode characteristics were in turn calculated from the flight derivatives.

THIS DOCUMENT PROVIDED BY THE ABBOTT AEROSPACE
TECHNICAL LIBRARY
ABBOTTAEROSPACE.COM

Most of the derivatives obtained showed consistent and generally normal variations with lift coefficient, Mach number, and altitude. Many of the derivatives showed well-defined effects due to flap deflection, notably those for spoiler effectiveness and directional stability.

The period, damping, and other mode shape characteristics calculated from the measured derivatives also exhibited normal trends with Mach number, altitude, and flap configuration.

The damping ratio of the short-period longitudinal mode was large, from 0.4 to 0.8, whereas the Dutch roll damping ratio for all conditions was light (less than 0.075) with the yaw damper off.

Flight Research Center,
National Aeronautics and Space Administration,
Edwards, Calif., December 7, 1971.

THIS DOCUMENT PROVIDED BY THE ABBOTT AEROSPACE
TECHNICAL LIBRARY
ABBOTTAEROSPACE.COM

APPENDIX A

EQUATIONS USED FOR FLIGHT DATA ANALYSIS

The equations of motion used to determine stability and control derivatives by the Newton-Raphson technique of matching flight data time histories are summarized in this appendix. The equations are in body-axes form.

Longitudinal Derivatives

The following equations were used to analyze longitudinal short-period maneuvers:

$$\dot{q} = M_\alpha \alpha + M_q q + M_{\delta_e} \delta_e$$

$$\dot{\alpha} = q - N_\alpha \alpha - N_q q - N_{\delta_e} \delta_e + \frac{g}{V_o}$$

$$a_n = \frac{V_o}{g}(N_\alpha \alpha + N_q q + N_{\delta_e} \delta_e)$$

$$\dot{\theta} = q$$

The zero shifts of q and a_n were determined in the Newton-Raphson program by using the same error minimization principle as used for finding the derivatives.

Position correction for instrument location was unnecessary for a_n, because the accelerometer was located at the center of gravity; however, the following equation was used to correct for the α-vane location:

$$\alpha = \alpha_i + \frac{x_\alpha}{V_o} q$$

The following expression was substituted for N_{δ_e} (see appendix B):

$$N_{\delta_e} = -\frac{I_Y g}{W V_o l} M_{\delta_e}$$

Lateral-Directional Derivatives

The analysis of lateral maneuver derivatives was based on the following equations:

THIS DOCUMENT PROVIDED BY THE ABBOTT AEROSPACE
TECHNICAL LIBRARY
ABBOTTAEROSPACE.COM

$$\dot{p} = \frac{I_{XZ}}{I_X}\dot{r} + L_p p + L_r r + L_\beta \beta + L_{\delta_a}\delta_a + L_{\delta_r}\delta_r + L_{\delta_s}\delta_s$$

$$\dot{r} = \frac{I_{XZ}}{I_Z}\dot{p} + N_p p + N_r r + N_\beta \beta + N_{\delta_a}\delta_a + N_{\delta_r}\delta_r + N_{\delta_s}\delta_s$$

$$\dot{\beta} = -r + \left(\frac{g}{V_o}\right)\varphi + p\alpha_o + Y_p p + Y_r r + Y_\beta \beta + Y_{\delta_a}\delta_a + Y_{\delta_r}\delta_r + Y_{\delta_s}\delta_s$$

$$a_t = \frac{V_o}{g}\left(Y_p p + Y_r r + Y_\beta \beta + Y_{\delta_a}\delta_a + Y_{\delta_r}\delta_r + Y_{\delta_s}\delta_s\right)$$

$$\dot{\varphi} = p + r\theta_o$$

Again, the error minimization principle used in the Newton-Raphson method to find the zero shifts of p and r was the same as that used to determine the derivatives.

Position correction for instrument location was not necessary for a_t because of the center-of-gravity location of the accelerometer; however, the following equation was used to correct for the β-vane location:

$$\beta = \beta_i - \frac{x_\beta}{V_o} r$$

THIS DOCUMENT PROVIDED BY THE ABBOTT AEROSPACE
TECHNICAL LIBRARY
ABBOTTAEROSPACE.COM

APPENDIX B

USE OF THE NEWTON-RAPHSON METHOD FOR DERIVATIVE DETERMINATION

Technique Used

The Newton-Raphson method of analysis (ref. 5) has many options to help the user to obtain the best possible set of derivatives with the flight data available. Primarily, these options permit control over which flight parameters (for example, p, r, β, q, α) are to be used in matching the time histories, what weight is to be attached to the flight parameters, and which of the derivatives should be allowed to vary from the initial starting values (usually wind-tunnel data or some reasonable estimate). The task of determining and assessing the effects of all combinations of different options for analyzing these data would be monumental; therefore, all the derivatives were allowed to vary and were weighted equally in the cost function. No attempt was made to control a particular derivative even if it appeared that the result could be improved by using other options.

The basic principle of the Newton-Raphson method of analysis is to minimize the error in a match between flight time histories and computed time histories on the basis of the estimated or calculated derivatives. Only short-duration inputs were used as forcing functions (pulses and doublets); thus the control derivatives determined were based on much less information than the remaining stability derivatives. Although the pulse and doublet maneuvers provided good time history matches and derivative results, the ideal maneuver for the Newton-Raphson matching process would contain continuous forcing of the controls, independent of the other variables to be matched.

Lift Due to Elevator

Initially, the control derivative, N_{δ_e}, was allowed to vary independently, but the results produced considerable scatter and obvious discrepancies in the calculated time histories. Therefore the derivative was assumed to be proportional to the elevator pitching moment, M_{δ_e}, according to the following expression inserted in the program for all longitudinal short-period matching:

$$N_{\delta_e} = -M_{\delta_e} \frac{I_Y g}{W V_o l}$$

Matching Multiple Time Histories

With the first version of the Newton-Raphson method used, only one maneuver at a time could be matched. It was observed that independent matching of the three maneuvers available at a particular flight condition often gave significantly different sets of derivatives. The difficulty was due primarily to the lack of sufficient dynamic information in any one maneuver. At this point the program was modified to match all

THIS DOCUMENT PROVIDED BY THE ABBOTT AEROSPACE
TECHNICAL LIBRARY
ABBOTTAEROSPACE.COM

three maneuvers simultaneously; the results showed much better consistency when the derivatives were compared with those obtained at other flight conditions. Figure 17 is a comparison of dimensional derivatives obtained by matching three maneuvers separately and then simultaneously. The derivatives L_p, L_r, N_p, and N_r show significant differences when matched separately. In all the matches the overall consistency of the derivatives increased when the three maneuvers were matched simultaneously.

Effect of Data Interval, $\Delta t = 0.1$ Versus 0.2

Shown also in figure 17 is a comparison of matches made at an available sample rate of 10 points per second and at the 5-point-per-second rate used throughout the lateral-directional analysis. The selection of 5 points per second was dictated by the limited amount of computer time available, and resulted in a reduction in computer time by approximately one-half. For all the derivatives the differences in the sampling rates are negligible, and the 5-point-per-second rate was adequate for the present investigation.

Effect of Principal-Axes Inclination

The basic computations in the Newton-Raphson method were performed in the principal axes for which the cross product of inertia, I_{XZ}, is zero. Because the manufacturer's estimates of the inertias of the CV-990 airplane, although limited, indicated a small I_{XZ}, the assumption was made that the inclination of the principal axes, ϵ, was zero for all time history matches. To verify this assumption, the effect of ϵ on the match of the time histories and the derivatives was checked. The flight parameters of roll rate and yaw rate were transformed from the aircraft body axes to the principal axes on the basis of assumed ϵ. The product of inertia is related to ϵ and the principal-axes-oriented moments of inertia by the following expression:

$$I_{XZ} = \frac{1}{2} (I_X - I_Z) \sin 2\epsilon$$

A complete set of derivatives was calculated for inclination angles of -2°, -1°, 0°, 1°, and 2° from two sets of maneuvers, selected for the extreme airplane weight differences, at the following flight conditions:

Speed	Altitude, m (ft)	Configuration	Weight, kg (lb)
140 knots	3,960 (13,000)	50° flaps	63,504 (140,000)
0.80 M	10,670 (35,000)	Clean	95,256 (210,000)

The effect of ϵ on the derivatives is shown in figure 18. The only derivative affected significantly for both flight conditions was L_p, which varied up to 10 percent per degree ϵ from the value obtained for $\epsilon = 0°$. The only other derivative affected appreciably was N_{δ_a}. In one maneuver set the N_{δ_a} derivative varied up to 12 percent per degree.

THIS DOCUMENT PROVIDED BY THE ABBOTT AEROSPACE
TECHNICAL LIBRARY
ABBOTTAEROSPACE.COM

The most likely value of ϵ was determined by plotting ϵ versus total error. The total error, which is the magnitude of the cost function at convergence, indicates the magnitude of the standard deviation between the flight data time history and its corresponding Newton-Raphson calculated match. An improved match with a smaller discrepancy between the time histories results in a reduction of the total error. The variation of total error with ϵ (fig. 19) tends to confirm the assumption that $I_{XZ} = 0$.

If all other data are considered to be good, theoretically, the total error should be minimal for each match. Therefore, the minimum total error defined by the variation in ϵ should also define the most probable values of ϵ and I_{XZ} of the airplane.

Because the minimization of ϵ occurred in the ϵ range of -1° to 1° (fig. 19), the assumption that $\epsilon \approx 0$ appears to be valid for all gross weights.

THIS DOCUMENT PROVIDED BY THE ABBOTT AEROSPACE
TECHNICAL LIBRARY
ABBOTTAEROSPACE.COM

REFERENCES

1. Kier, David A.: Flight Comparison of Several Techniques for Determining the Minimum Flying Speed for a Large, Subsonic Jet Transport. NASA TN D-5806, 1970.

2. Adkins, Elmor J.; McLeod, Norman J.; and Lasagna, Paul L.: Variation in Engine Noise for Two Landing-Approach Configurations of a Jet Transport Aircraft. NASA TM X-1896, 1969.

3. Holleman, Euclid C.; and Gilyard, Glenn B.: In-Flight Evaluations of the Lateral Handling of a Four-Engine Jet Transport During Approach and Landing. NASA TN D-6339, 1971.

4. Holleman, Euclid C.; and Gilyard, Glenn B.: In-Flight Pilot Evaluations of the Flying Qualities of a Four-Engine Jet Transport. NASA TN D-6811, 1972.

5. Iliff, Kenneth W.; and Taylor, Lawrence W., Jr.: Determination of Stability Derivatives From Flight Data Using a Newton-Raphson Minimization Technique. NASA TN D-6579, 1972.

6. Mechtly, E. A.: The International System of Units - Physical Constants and Conversion Factors. NASA SP-7012, 1969.

7. Wolowicz, Chester H.: Considerations in the Determination of Stability and Control Derivatives and Dynamic Characteristics From Flight Data. AGARD Rep. 549 - Part 1, 1966.

THIS DOCUMENT PROVIDED BY THE ABBOTT AEROSPACE
TECHNICAL LIBRARY
ABBOTTAEROSPACE.COM

TABLE 1.– PHYSICAL CHARACTERISTICS OF THE CV-990 AIRPLANE

Fuselage –	
Maximum width, m (ft)	3.51 (11.50)
Maximum height, m (ft)	3.78 (12.42)
Length, m (ft)	42.60 (139.75)
Wing –	
Incidence (root), deg	4
Aerodynamic span, m (ft)	35.97 (117.99)
Area, m^2 (ft^2)	209 (2250)
Root chord, m (ft)	8.25 (27.06)
Tip chord, m (ft)	2.69 (8.83)
Mean aerodynamic chord, m (ft)	6.34 (20.81)
Dihedral, deg	7
Aspect ratio	6.2
Leading-edge sweep, deg	39
Horizontal tail –	
Area, m^2 (ft^2)	39.6 (426.55)
Dihedral, deg	7.5
Leading-edge sweep, deg	41
Span, m (ft)	11.80 (38.74)
Aspect ratio	3.52
Vertical tail –	
Area, m^2 (ft^2)	27.4 (295)
Sweep at 30-percent chord, deg	35
Span, m (ft)	6.45 (21.17)
Aspect ratio	1.52
Aileron –	
Area, m^2 (ft^2)	2.78 (29.97)
Span, m (ft)	2.93 (9.62)
Maximum travel, deg	±15
Inboard spoiler –	
Area, m^2 (ft^2)	1.65 (17.8)
Mean aerodynamic chord, m (ft)	0.85 (2.8)
Maximum travel, deg	75
Outboard spoiler –	
Area, m^2 (ft^2)	3.86 (41.51)
Mean aerodynamic chord, m (ft)	0.95 (3.11)
Maximum travel, deg	60

THIS DOCUMENT PROVIDED BY THE ABBOTT AEROSPACE
TECHNICAL LIBRARY
ABBOTTAEROSPACE.COM

TABLE 2.– CV-990 STABILITY AND CONTROL INSTRUMENTATION

Parameter	Range	Total error
Left-hand elevator	12.1° to -25.2°	1.8°
Right-hand elevator	11.4° to -25.7°	1.7°
Rudder	±25.1°	1.4°
Left-hand aileron	14.6° to -15°	1.4°
Right-hand aileron	15.1° to -16°	1.5°
Left-hand outboard spoiler	59.4° to 0°	2.6°
Left-hand inboard spoiler	68° to 0°	2.9°
Right-hand outboard spoiler	58.3° to 0°	2.6°
Right-hand inboard spoiler	73.2° to 0°	3.1°
Static pressure	15,082 N/m^2 (315 lb/ft^2)	891 N/m^2 (18.6 lb/ft^2)
Total pressure	3400 N/m^2 (71 lb/ft^2))	168 N/m^2 (3.5 lb/ft^2)
Angle of attack	35° to -15°	2.1°
Angle of sideslip	±16°	1.4°
Pitch angle	40° to -20°	2.7°
Roll angle	±20°	1.9°
Pitch rate	±10 deg/sec	.9 deg/sec
Roll rate	±20 deg/sec	1.8 deg/sec
Yaw rate	±10 deg/sec	.9 deg/sec
Center-of-gravity normal acceleration	2.5g to 0 g	.11g
Center-of-gravity transverse acceleration	±.5g	.04g

TABLE 3.– CV-990 BASIC FLIGHT CONDITIONS

(a) Longitudinal

V_i, knots or M	h_p, m (ft)	δ_f, deg	Gear position	W, kg (lb)	Center of gravity, percent $\bar{c}$	α_{trim}, deg	I_Y, kg-m^2 (slug-ft^2)
120	3,960 (13,000)	50	Down	0.5988×10^5 (1.32×10^5)	24.8	8.2	5.545×10^6 (4.090×10^6)
120	3,960 (13,000)	27	Down	.6305 (1.39)	24.7	11.1	5.410 (3.990)
140	3,960 (13,000)	50	Down	.6623 (1.46)	24.9	4.9	5.274 (3.890)
140	3,500 (11,500)	27	Down	.6623 (1.46)	24.4	7.4	5.274 (3.890)
160	3,960 (13,000)	50	Down	.6713 (1.48)	24.2	2.6	5.274 (3.890)
160	3,960 (13,000)	27	Down	.7122 (1.57)	23.4	5.2	5.139 (3.790)
180	3,960 (13,000)	50	Down	.7666 (1.69)	24.3	1.3	4.976 (3.670)
180	3,960 (13,000)	27	Down	.8187 (1.81)	23.8	4.0	4.867 (3.590)
192	4,570 (15,000)	27	Down	.6895 (1.52)	24.2	.6	5.026 (3.840)
195	4,570 (15,000)	0	Down	.7303 (1.61)	24.5	4.2	5.057 (3.730)
195	3,960 (13,000)	0	Up	.6486 (1.43)	24.4	3.0	5.342 (3.940)
.40	6,096 (20,000)	0	Up	.7530 (1.66)	25.3	6.3	4.976 (3.670)
.50	6,250 (20,500)	0	Up	.8074 (1.78)	25.4	3.4	4.840 (3.570)
.60	6,096 (20,000)	0	Up	.8709 (1.92)	26.5	1.5	4.718 (3.480)
.70	6,096 (20,000)	0	Up	.9707 (2.14)	20.5	1.0	4.935 (3.640)
.80	6,130 (20,100)	0	Up	.7620 (1.68)	20.4	-.7	5.003 (3.690)
.85	6,400 (21,000)	0	Up	.7439 (1.64)	23.8	-.8	5.030 (3.710)
.70	8,534 (28,000)	0	Up	.7802 (1.72)	23.8	.7	4.949 (3.650)
.61	10,670 (35,000)	0	Up	.9163 (2.02)	24.2	5.6	4.786 (3.530)
.70	10,670 (35,000)	0	Up	.9435 (2.08)	22.2	3.3	4.867 (3.590)
.80	10,670 (35,000)	0	Up	.9616 (2.12)	22.1	1.8	4.895 (3.610)
.87	10,670 (35,000)	0	Up	.7847 (1.73)	24.3	.8	4.935 (3.640)

THIS DOCUMENT PROVIDED BY THE ABBOTT AEROSPACE TECHNICAL LIBRARY ABBOTTAEROSPACE.COM

TABLE 3.– Concluded

(b) Lateral-Directional

V_i, knots or M	h_p, m (ft)	δ_f, deg	Gear	W, kg (lb)	Center of gravity, percent $\bar{c}$	α_{trim}, deg	I_X, kg-m^2 (slug-ft^2)	I_Z, kg-m^2 (slug-ft^2)
120	3,960 (13,000)	50	Down	0.5864×10^5 (1.29×10^5)	24.9	8.2	2.373×10^6 (1.750×10^6)	7.525×10^6 (5.550×10^6)
120	3,960 (13,000)	27	Down	.6136 (1.35)	24.8	11.1	2.386 (1.760)	7.525 (5.550)
140	3,960 (13,000)	50	Down	.6455 (1.42)	24.7	4.9	2.413 (1.780)	7.525 (5.550)
140	3,930 (12,900)	27	Down	.6455 (1.42)	24.5	7.4	2.427 (1.790)	7.525 (5.550)
160	3,960 (13,000)	50	Down	.6515 (1.43)	24.3	2.6	2.435 (1.796)	7.525 (5.550)
160	3,960 (13,000)	27	Down	.6970 (1.53)	23.8	5.2	2.503 (1.846)	7.538 (5.560)
175	3,730 (12,260)	50	Down	.7409 (1.63)	24.2	1.3	2.590 (1.910)	7.538 (5.560)
180	3,960 (13,000)	27	Down	.7924 (1.74)	24.9	4.0	2.725 (2.010)	7.565 (5.580)
195	4,570 (15,000)	27	Down	.6788 (1.49)	24.2	.6	2.468 (1.820)	7.560 (5.576)
194	4,860 (16,000)	0	Down	.7045 (1.55)	24.8	4.2	2.535 (1.870)	7.538 (5.560)
195	3,960 (13,000)	0	Up	.6545 (1.44)	24.5	3.0	2.427 (1.790)	7.525 (5.550)
.40	6,096 (20,000)	0	Up	.7515 (1.65)	25.4	6.3	2.617 (1.930)	7.525 (5.550)
.50	6,250 (20,500)	0	Up	.7909 (1.74)	25.4	3.4	2.725 (2.010)	7.538 (5.560)
.60	6,096 (20,000)	0	Up	.8500 (1.87)	24.2	1.5	2.915 (2.150)	7.633 (5.630)
.70	6,096 (20,000)	0	Up	.9530 (2.10)	21.5	1.0	3.272 (2.413)	7.932 (5.850)
.80	6,200 (20,300)	0	Up	.7500 (1.65)	23.9	-.7	2.617 (1.930)	7.552 (5.570)
.85	6,096 (20,000)	0	Up	.7242 (1.59)	23.9	-.8	2.549 (1.880)	7.552 (5.570)
.70	8,534 (28,000)	0	Up	.7773 (1.71)	24.1	.7	2.685 (1.980)	7.565 (5.580)
.61	10,350 (34,000)	0	Up	.9121 (2.01)	24.8	5.0	3.132 (2.310)	7.715 (5.690)
.70	10,670 (35,000)	0	Up	.9288 (2.04)	23.8	3.3	3.190 (2.353)	7.773 (5.733)
.80	10,670 (35,000)	0	Up	.9530 (2.10)	22.4	1.8	3.268 (2.410)	7.864 (5.800)
.86	10,670 (35,000)	0	Up	.7818 (1.72)	24.3	.8	2.712 (2.000)	7.552 (5.570)

THIS DOCUMENT PROVIDED BY THE ABBOTT AEROSPACE TECHNICAL LIBRARY ABBOTTAEROSPACE.COM

THIS DOCUMENT PROVIDED BY THE ABBOTT AEROSPACE
TECHNICAL LIBRARY
ABBOTTAEROSPACE.COM

TABLE 4.– VARIANCE AND PROBABLE-ERROR INDEX

Derivative	Variance	Probable-error index
Longitudinal		
M_q, 1/sec	0.0418	4.6
M_α, 1/sec^2	.0307	1.6
M_{δ_e}, 1/sec^2	.0401	2.3
N_q	.0110	---
N_α, 1/sec	.0138	3.8
Lateral-directional		
L_{δ_a}, 1/sec^2	0.00993	2.1
L_{δ_r}, 1/sec^2	.04199	13.1
L_{δ_s}, 1/sec^2	.01270	2.0
L_p, 1/sec	.01423	1.4
L_r, 1/sec	.02783	----
L_β, 1/sec^2	.04370	1.1
N_{δ_a}, 1/sec^2	.00143	2.2
N_{δ_r}, 1/sec^2	.00854	1.0
N_{δ_s}, 1/sec^2	.00189	1.9
N_p, 1/sec	.00226	----
N_r, 1/sec	.00447	5.2
N_β, 1/sec^2	.00505	.6
Y_{δ_a}, 1/sec	.00095	----
Y_{δ_r}, 1/sec	.00333	10.7
Y_{δ_s}, 1/sec	.00057	----
Y_β, 1/sec	.00189	1.3

TABLE 5.– CV-990 DIMENSIONAL DERIVATIVES

(a) Longitudinal

V_i, knots or M	h_p, m (ft)	δ_f, deg	Gear position	M_q	M_α	M_{δ_e}	N_q	N_α	N_{δ_e}
120	3,960 (13,000)	50	Down	-0.2145	-0.6565	-0.3380	0.50650	0.1055	0.0162383
120	3,960 (13,000)	27	Down	-.8580	-.4658	-.6478	.43375	.2788	.0300462
140	3,960 (13,000)	50	Down	-.8932	-.7798	-.8534	.15999	.4866	.0326879
140	3,500 (11,500)	27	Down	-.9558	-.4242	-.7943	.38161	.3287	.0311762
160	3,960 (13,000)	50	Down	-.9311	-1.1545	-1.1634	.16770	.7561	.0382597
160	3,960 (13,000)	27	Down	-1.0080	-1.0968	-1.1213	.16449	.6032	.0360433
180	3,960 (13,000)	50	Down	-1.0126	-1.2876	-1.2756	.06166	.6538	.0352414
180	3,960 (13,000)	27	Down	-1.0714	-1.4404	-1.4279	.04234	.6169	.0371148
192	4,570 (15,000)	27	Down	-.9587	-1.9121	-1.5927	.08736	.7617	.0420119
195	4,570 (15,000)	0	Down	-1.1732	-1.5000	-1.7419	.07981	.6512	.0435265
195	3,960 (13,000)	0	Up	-1.2037	-1.3451	-1.5872	.10552	.6690	.0429979
.40	6,096 (20,000)	0	Up	-.7357	-.6165	-1.3003	.04966	.4591	.0318525
.50	6,250 (20,500)	0	Up	-.9616	-1.2555	-1.6883	.11127	.5807	.0316784
.60	6,096 (20,000)	0	Up	-.8909	-2.6334	-2.4957	.00217	.7528	.0370859
.70	6,096 (20,000)	0	Up	-1.3338	-5.7575	-4.0053	-.00503	.8857	.0477859
.80	6,130 (20,100)	0	Up	-2.0696	-5.0671	-4.6495	-.01048	1.1349	.0564648
.85	6,400 (21,000)	0	Up	-2.4363	-6.4589	-5.2787	-.04713	1.2873	.0614508
.70	8,534 (28,000)	0	Up	-1.3521	-3.4328	-2.7112	.00529	.8061	.0382632
.61	10,670 (35,000)	0	Up	-.6642	-.4343	-1.5844	.03452	.2564	.0238488
.70	10,670 (35,000)	0	Up	-.8274	-1.0372	-1.7183	.04409	.3721	.0221392
.80	10,670 (35,000)	0	Up	-1.7511	-2.8908	-3.4395	.00716	.6686	.0383703
.87	10,670 (35,000)	0	Up	-1.3689	-4.6220	-2.7370	-.00247	.7899	.0318854

THIS DOCUMENT PROVIDED BY THE ABBOTT AEROSPACE TECHNICAL LIBRARY ABBOTTAEROSPACE.COM

TABLE 5.– Concluded

(b) Lateral-directional

V_i, knots or M	h_p, m (ft)	δ_f, deg	Gear	L_p	L_r	L_β	$L\delta_a$	$L\delta_r$	$L\delta_s$	N_p	N_r	N_β	$N\delta_a$	$N\delta_r$	$N\delta_s$	Y_β	$Y\delta_a$	$Y\delta_r$	$Y\delta_s$
120	3,960 (13,000)	50	Down	-0.662	0.499	-1.587	0.188	0.070	0.425	-0.113	-0.089	0.323	0.0525	-0.342	0.0915	-0.125	-0.0083	0.035	0.0019
120	3,960 (13,000)	27	Down	-.766	.257	-1.755	.153	.092	.258	-.141	-.121	.202	.0506	-.305	.0652	-.123	-.0052	.044	.0031
140	3,960 (13,000)	50	Down	-.838	.325	-2.063	.235	.210	.509	-.087	-.116	.522	.0546	-.424	.1134	-.146	-.0108	.022	-.0006
140	3,930 (12,900)	27	Down	-.918	-.059	-2.037	.294	.131	.350	-.104	-.116	.414	.0498	-.439	.0804	-.124	-.0025	.007	-.0069
160	3,960 (13,000)	50	Down	-.950	.216	-2.357	.374	.153	.631	-.056	-.089	.727	.0458	-.483	.1606	-.159	-.0060	.029	-.0024
160	3,960 (13,000)	27	Down	-.927	.185	-2.246	.349	.344	.394	-.111	-.130	.514	.0766	-.509	.0945	-.137	-.0009	.024	-.0013
175	3,730 (12,260)	50	Down	-.899	.280	-2.311	.401	.188	.694	-.067	-.152	.839	.0689	-.597	.1540	-.151	.0011	.023	-.0046
180	3,960 (13,000)	27	Down	-1.002	.027	-2.405	.420	.227	.433	-.082	-.136	.692	.0878	-.584	.1220	-.143	.0006	.027	-.0025
195	4,570 (15,000)	27	Down	-1.139	-.095	-2.774	.571	.113	.628	-.074	-.084	.965	.1138	-.709	.1448	-.160	-.0040	.040	-.0015
194	4,860 (16,000)	0	Down	-1.011	.002	-3.328	.572	.171	.369	-.082	-.136	.812	.0848	-.722	.0683	-.161	.0020	.035	.0004
195	3,960 (13,000)	0	Up	-1.195	-.047	-3.175	.551	.369	.549	-.058	-.123	.972	.0902	-.849	.0612	-.157	.0025	.033	.0027
.40	6,096 (20,000)	0	Up	-.790	.139	-2.602	.400	.262	.262	-.091	-.124	.582	.0600	-.656	.0528	-.111	0	.028	-.0008
.50	6,250 (20,500)	0	Up	-.862	.174	-3.003	.600	.530	.458	-.054	-.068	1.011	.0700	-.873	.0660	-.124	0	.023	.0027
.60	6,096 (20,000)	0	Up	-1.077	-.106	-4.063	.900	.810	.620	-.024	-.096	1.613	.0900	-1.207	.1190	-.143	.0040	.040	-.0013
.70	6,096 (20,000)	0	Up	-1.274	-.549	-5.142	1.300	.369	.961	-.014	-.118	2.289	.1201	-1.615	.1400	-.148	.0070	.035	-.0018
.80	6,200 (20,300)	0	Up	-1.570	.036	-7.234	1.847	2.586	1.274	.020	-.103	3.470	.1652	-1.808	.1329	-.230	.0079	.052	-.0030
.85	6,096 (20,000)	0	Up	-1.748	.123	-8.455	2.252	.822	1.011	.045	-.068	4.027	.1873	-1.713	.1418	-.259	.0069	.033	.0004
.70	8,534 (28,000)	0	Up	-1.182	-.122	-4.926	1.203	.681	.783	-.013	-.088	1.869	.1305	-1.161	.1054	-.154	.0035	.034	.0005
.61	10,350 (34,000)	0	Up	-.503	-.070	-2.584	.436	.160	.229	-.027	-.058	.682	.0562	-.655	.0516	-.073	-.0025	.015	.0007
.70	10,670 (35,000)	0	Up	-.724	.051	-3.429	.702	.278	.488	-.039	-.029	1.036	.0897	-.756	.0699	-.089	.0036	.024	-.0023
.80	10,670 (35,000)	0	Up	-.814	-.100	-4.166	.996	-.005	.685	-.068	-.154	1.475	.1447	-1.158	.1019	-.097	.0017	.015	-.0013
.86	10,670 (35,000)	0	Up	-1.144	-.371	-4.990	1.300	.912	.789	-.011	-.098	2.270	.1900	-1.335	.1063	-.130	0	.023	-.0007

THIS DOCUMENT PROVIDED BY THE ABBOTT AEROSPACE
TECHNICAL LIBRARY
ABBOTTAEROSPACE.COM

This Document Provided by the Abbott Aerospace
Technical Library
abbottaerospace.com

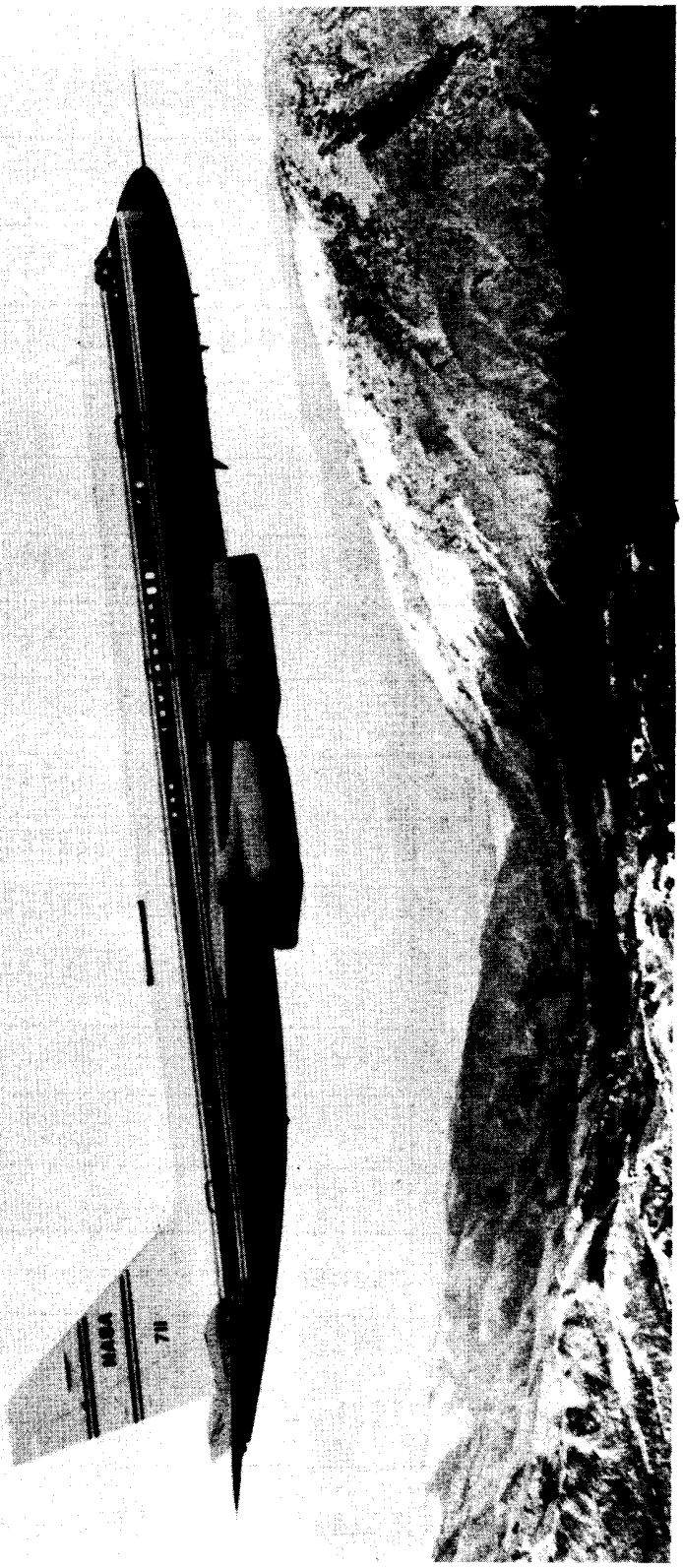

E-19752

Figure 1. CV-990 airplane.

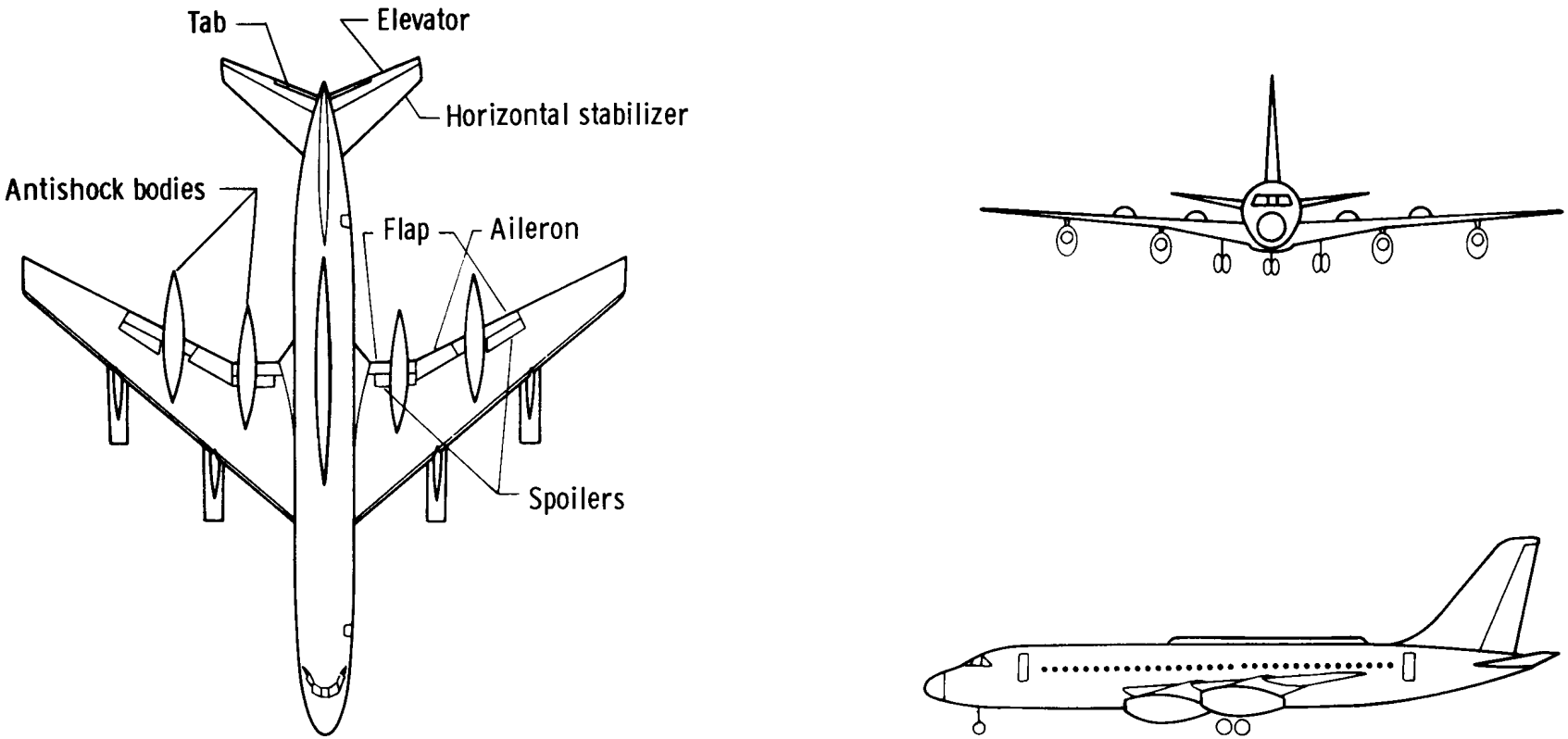

Figure 2. Three-view sketch of the CV-990 airplane.

THIS DOCUMENT PROVIDED BY THE ABBOTT AEROSPACE
TECHNICAL LIBRARY
ABBOTTAEROSPACE.COM

THIS DOCUMENT PROVIDED BY THE ABBOTT AEROSPACE
TECHNICAL LIBRARY
ABBOTTAEROSPACE.COM

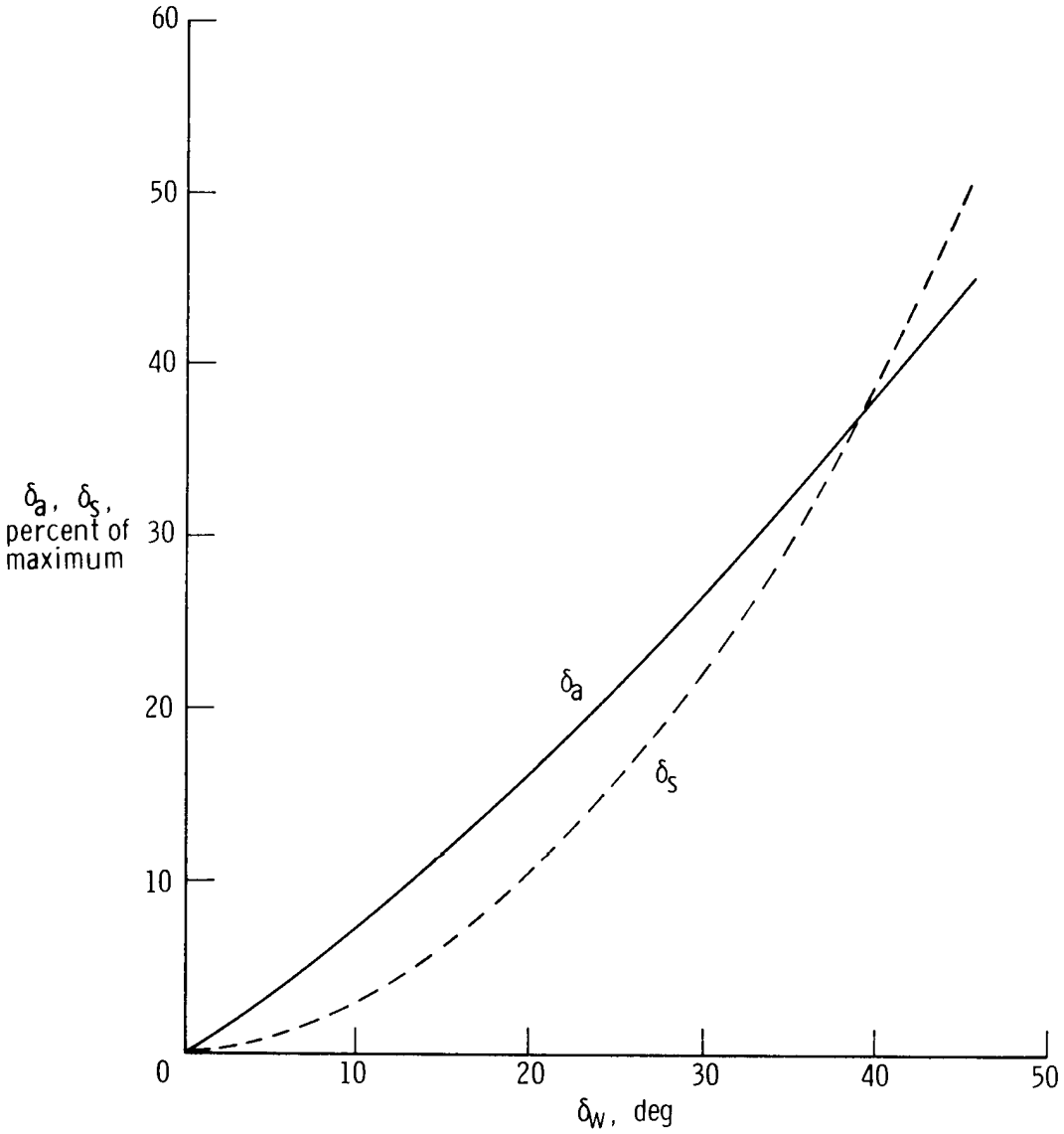

Figure 3. Variation of aileron and spoiler deflection with the normal range of wheel usage.

THIS DOCUMENT PROVIDED BY THE ABBOTT AEROSPACE
TECHNICAL LIBRARY
ABBOTTAEROSPACE.COM

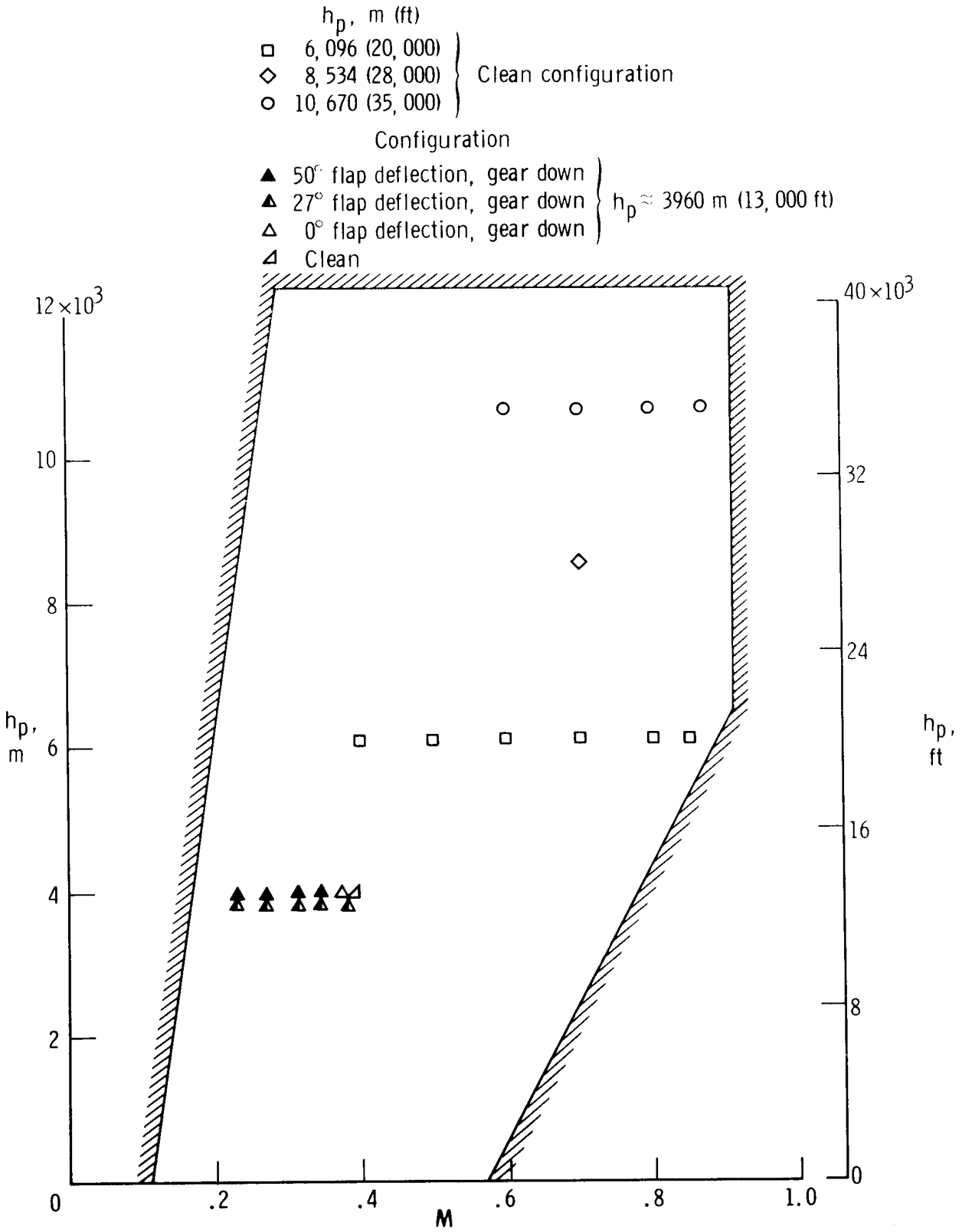

Figure 4. CV-990 operating envelope showing Mach number and altitude conditions at which stability and control data were obtained.

THIS DOCUMENT PROVIDED BY THE ABBOTT AEROSPACE
TECHNICAL LIBRARY
ABBOTTAEROSPACE.COM

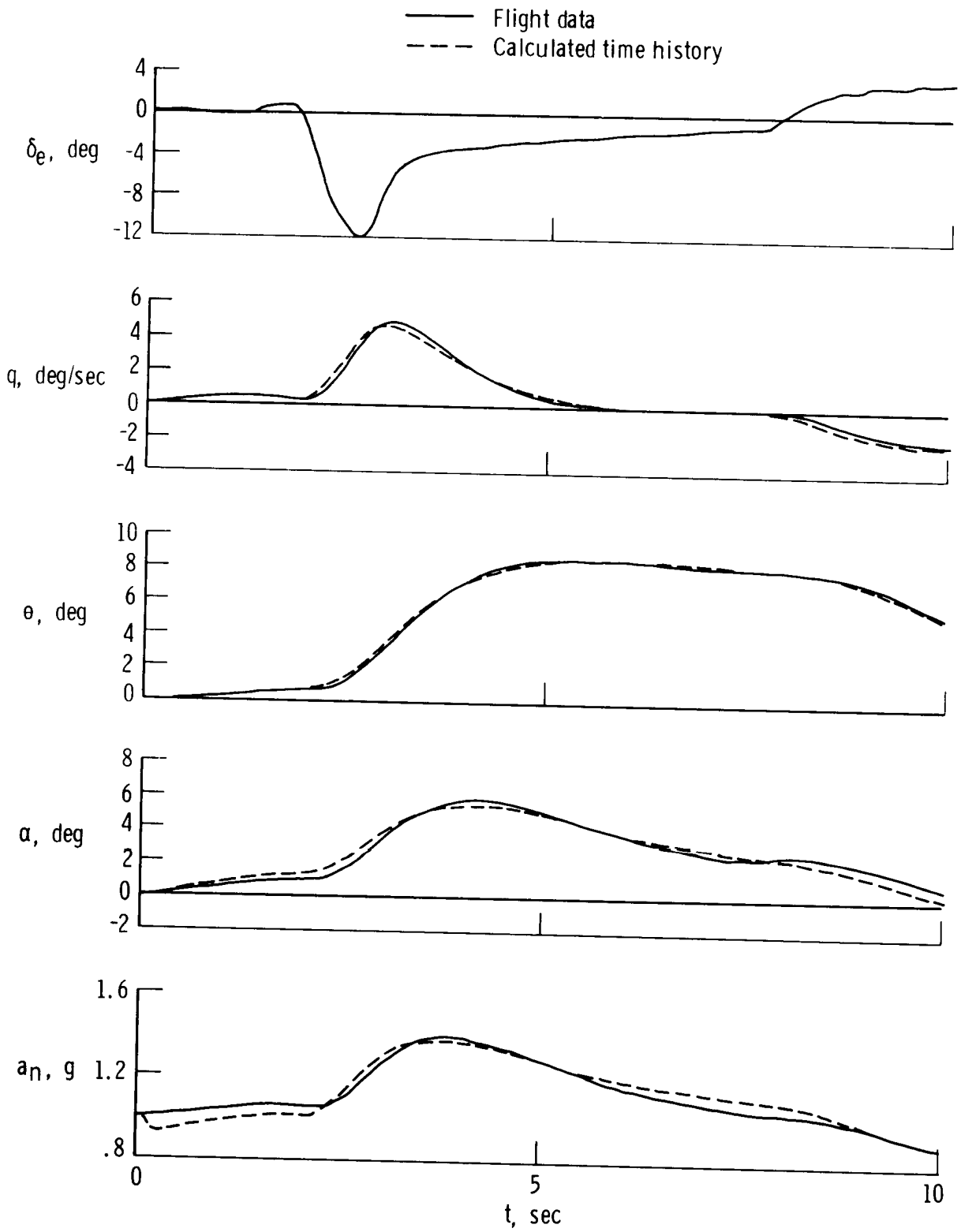

(a) V_i = 140 knots, h_p = 3960 m (13,000 ft), δ_f = 50°.

Figure 5. Typical Newton-Raphson matches of pullup and release maneuver time histories.

This Document Provided by the Abbott Aerospace
Technical Library
abbottaerospace.com

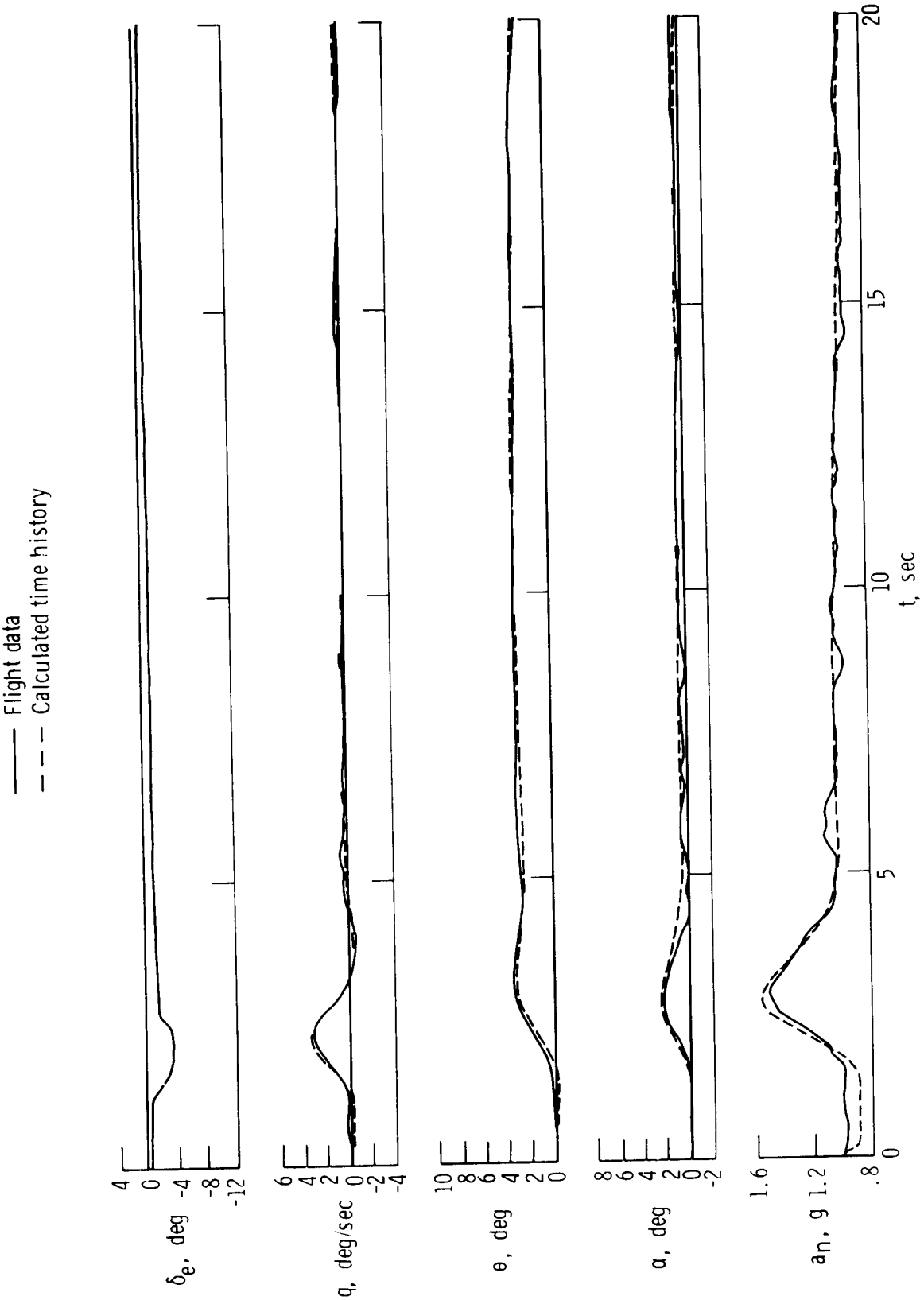

(b) M = 0.80, h_p = 10,670 m (35,000 ft), clean configuration.

Figure 5. Concluded.

THIS DOCUMENT PROVIDED BY THE ABBOTT AEROSPACE
TECHNICAL LIBRARY
ABBOTTAEROSPACE.COM

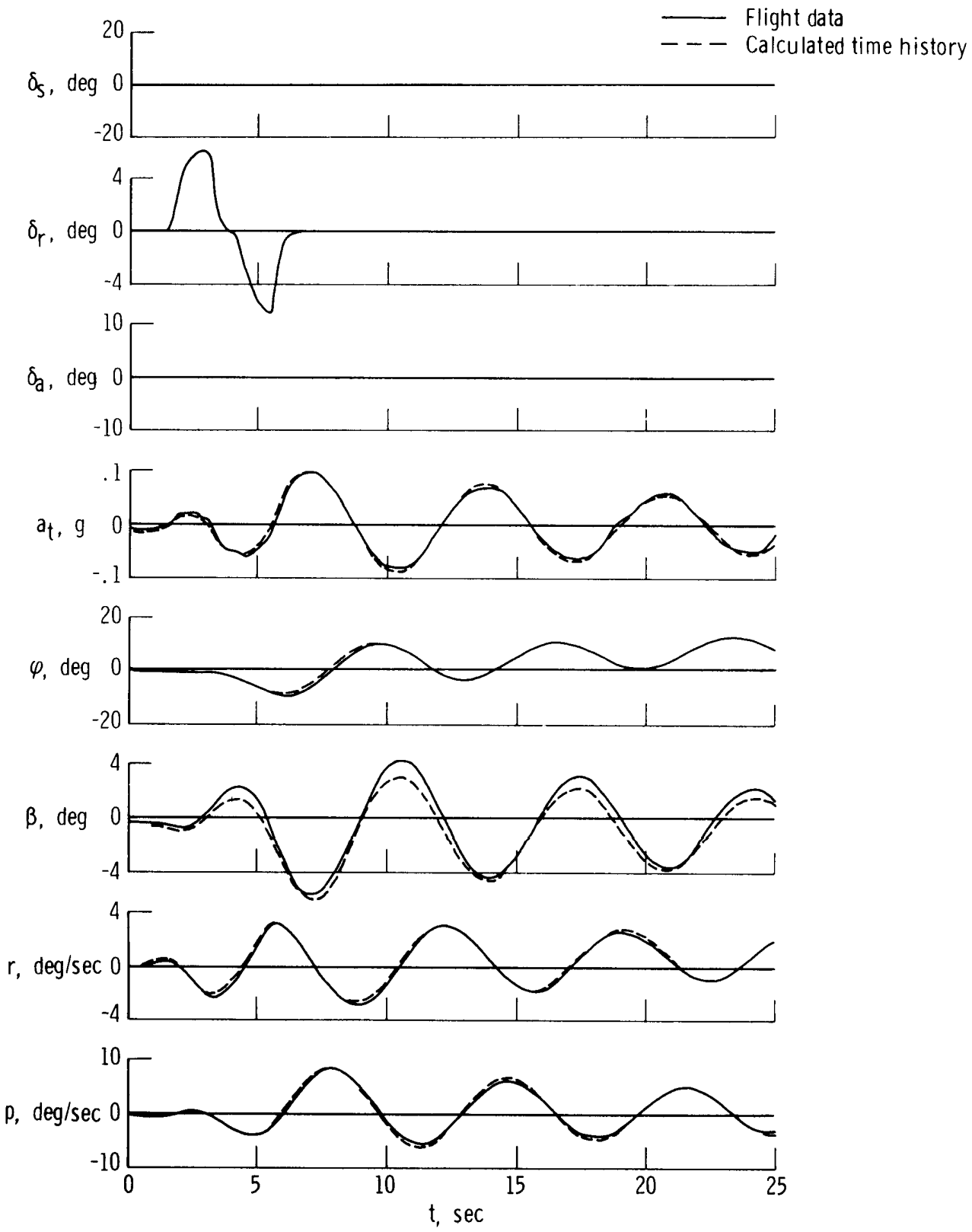

(a) Rudder doublet: V_i = 140 knots, h_p = 3960 m (13,000 ft), δ_f = 50°.

Figure 6. Typical Newton-Raphson matches of lateral-directional maneuver time histories.

THIS DOCUMENT PROVIDED BY THE ABBOTT AEROSPACE
TECHNICAL LIBRARY
ABBOTTAEROSPACE.COM

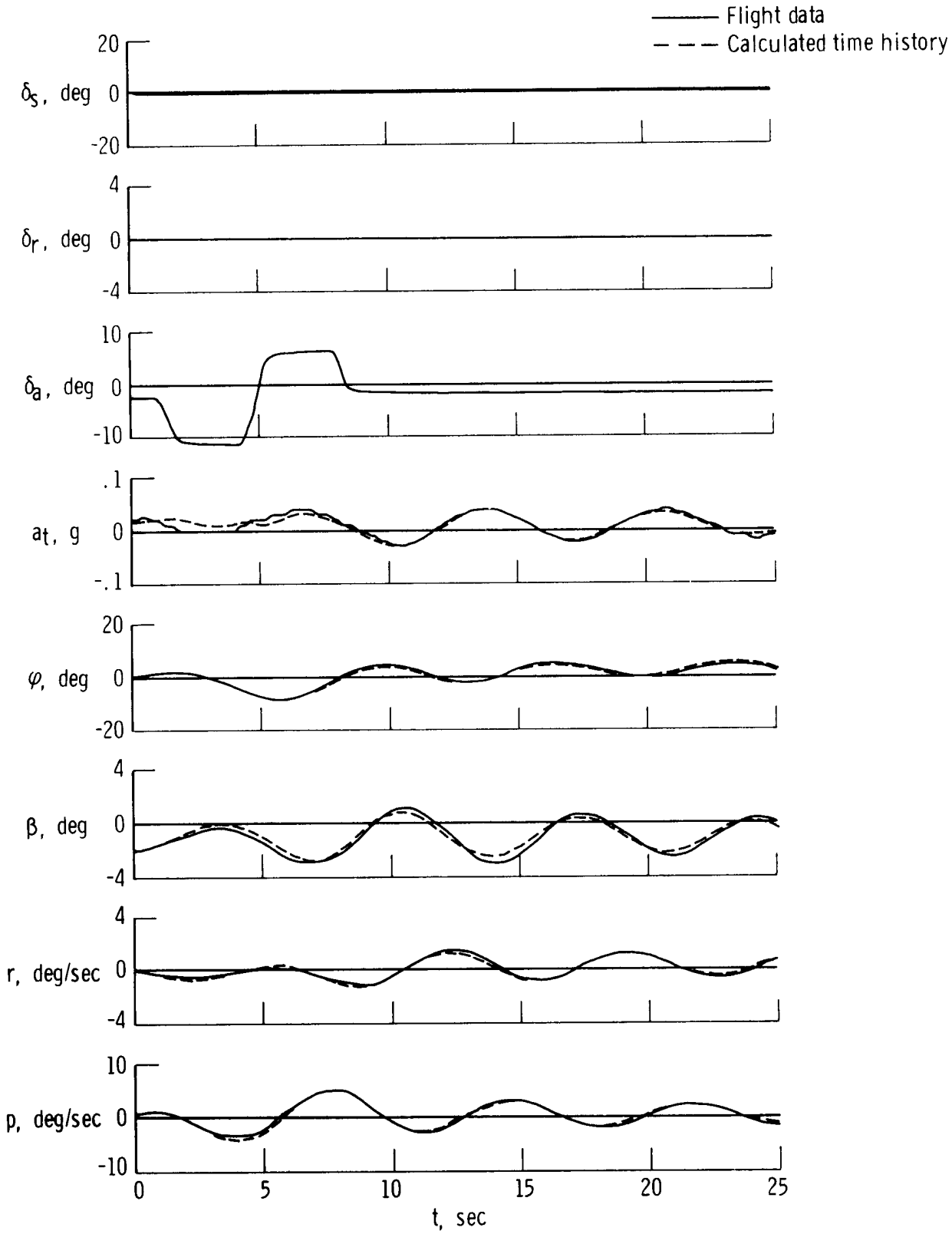

(b) Aileron doublet: V_i = 140 knots, h_p = 3960 m (13,000 ft), $\delta_f = 50°$.

Figure 6. Continued.

THIS DOCUMENT PROVIDED BY THE ABBOTT AEROSPACE
TECHNICAL LIBRARY
ABBOTTAEROSPACE.COM

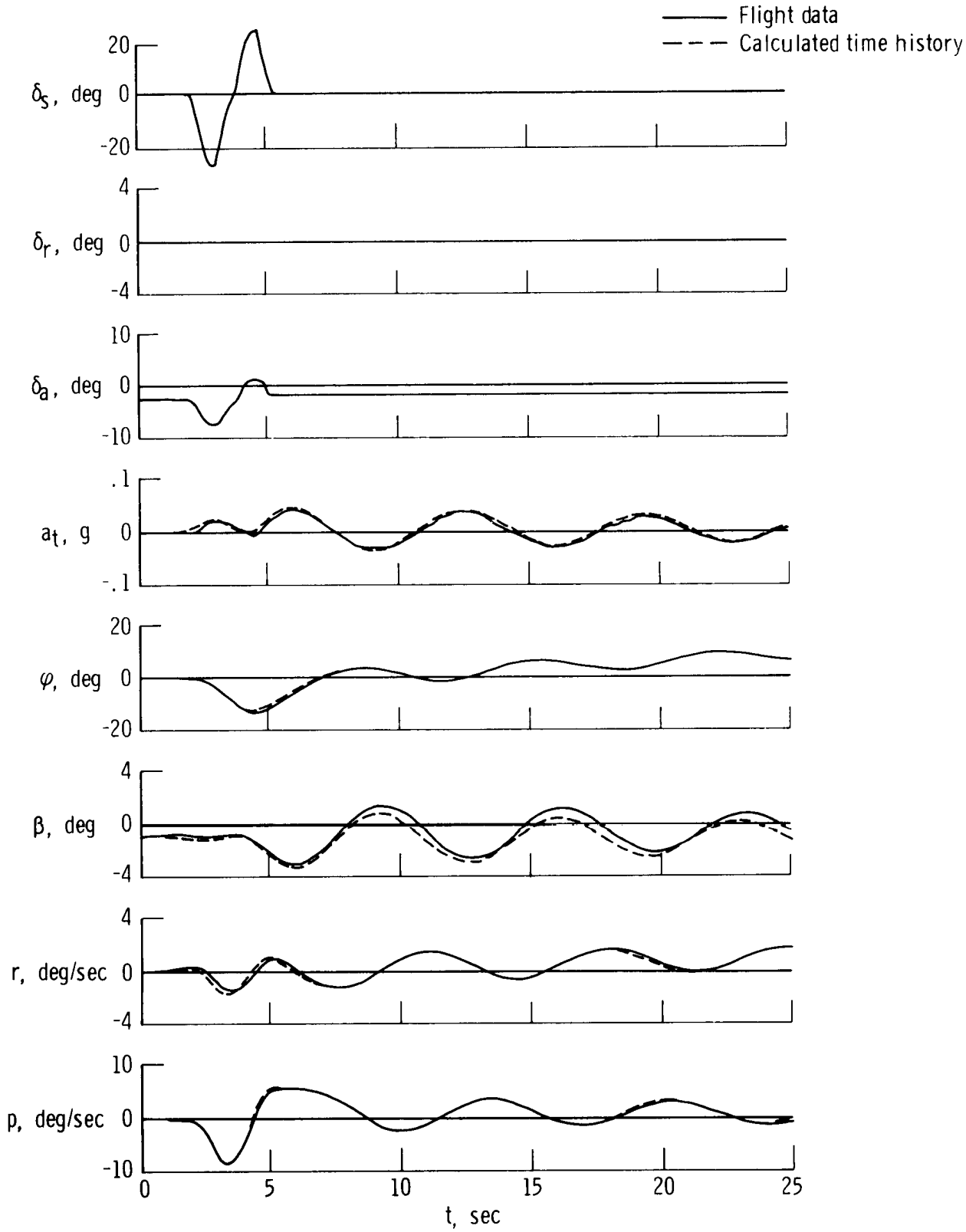

(c) Aileron plus spoiler doublet: V_i = 140 knots, h_p = 3960 m (13,000 ft), $\delta_f = 50°$.

Figure 6. Continued.

THIS DOCUMENT PROVIDED BY THE ABBOTT AEROSPACE
TECHNICAL LIBRARY
ABBOTTAEROSPACE.COM

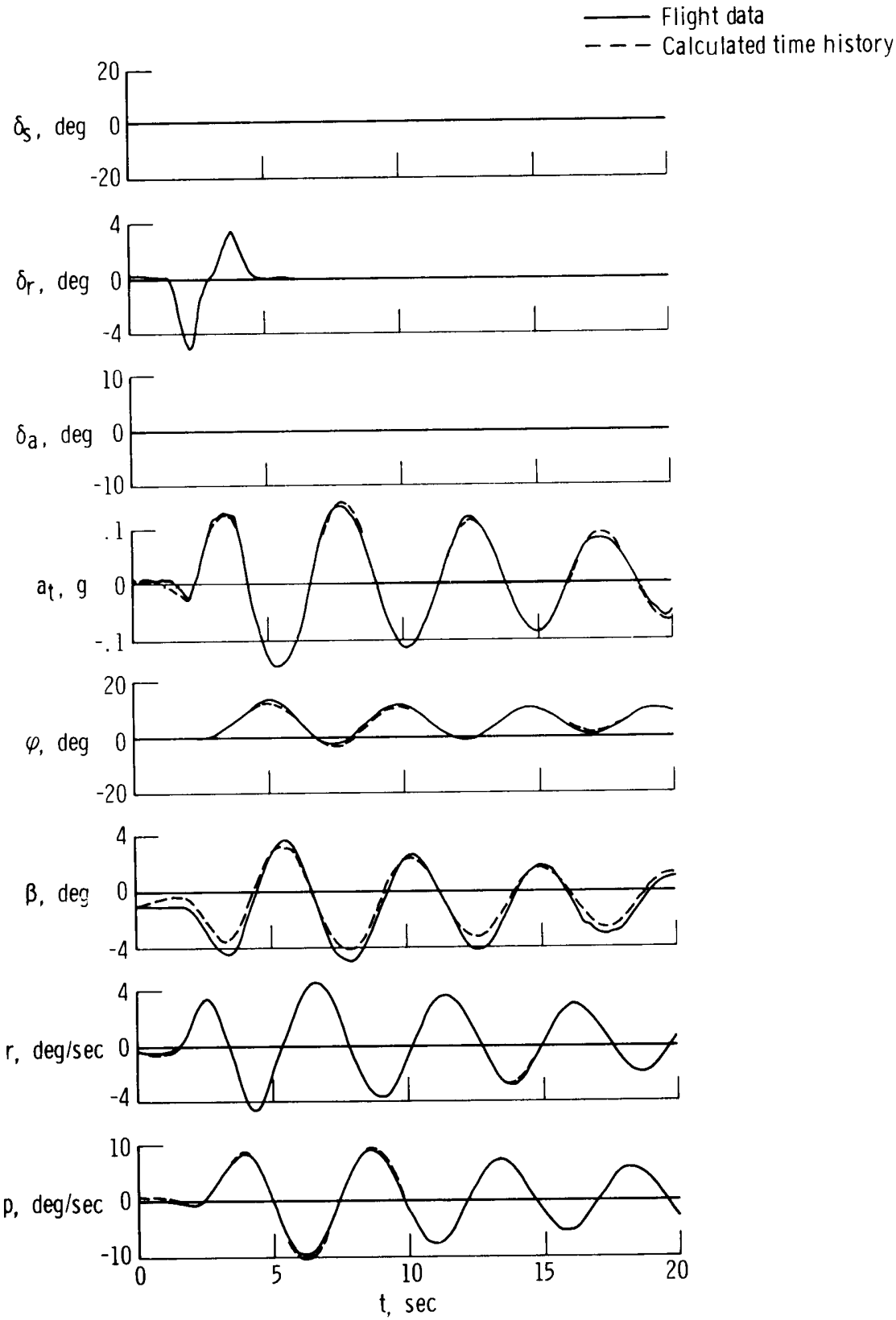

(d) Rudder doublet: M = 0.80, h_p = 10,670 m (35,000 ft), clean configuration.

Figure 6. Continued.

THIS DOCUMENT PROVIDED BY THE ABBOTT AEROSPACE
TECHNICAL LIBRARY
ABBOTTAEROSPACE.COM

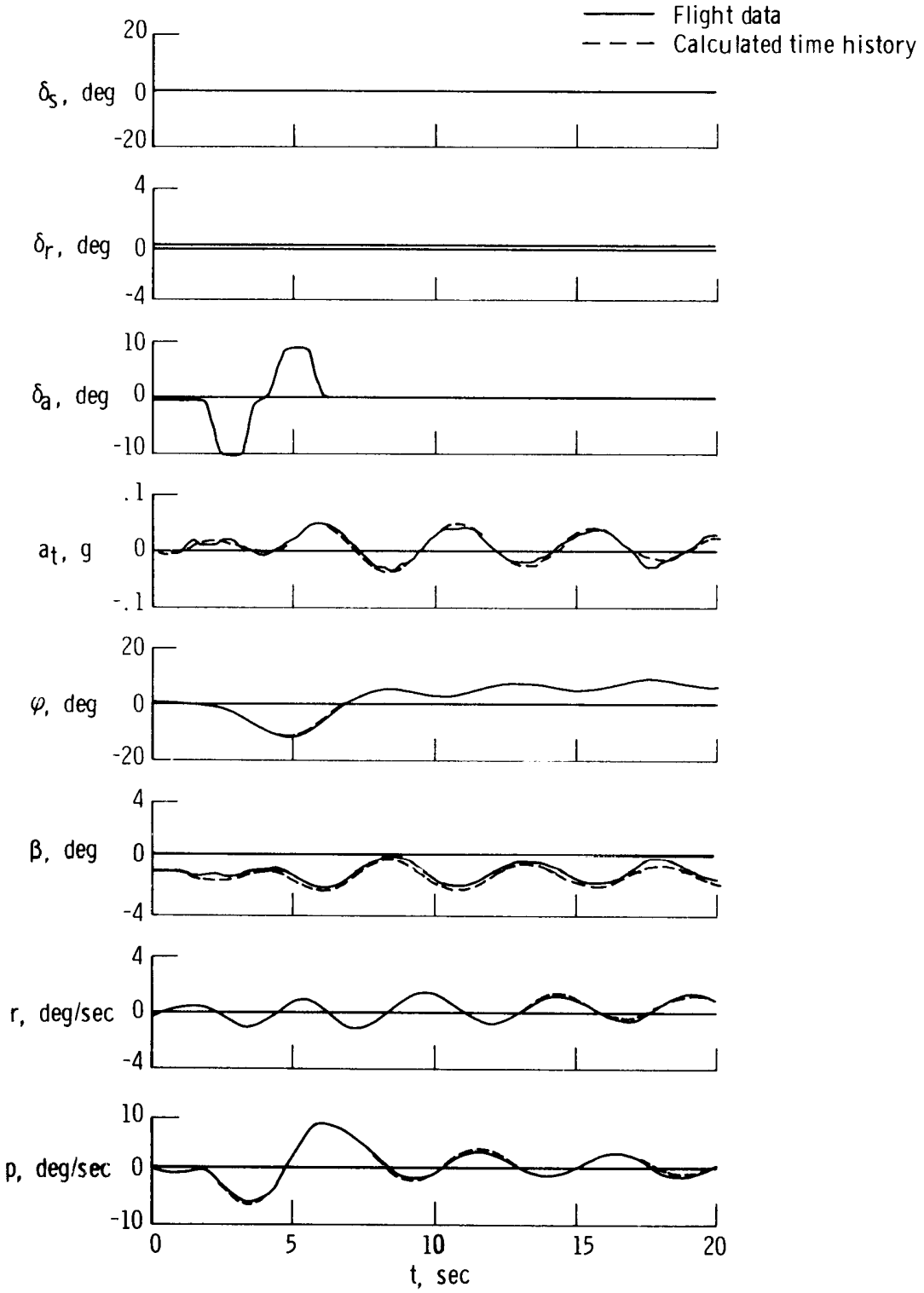

(e) Aileron doublet: M = 0.80, h_p = 10,670 m (35,000 ft), clean configuration.

Figure 6. Continued.

THIS DOCUMENT PROVIDED BY THE ABBOTT AEROSPACE
TECHNICAL LIBRARY
ABBOTTAEROSPACE.COM

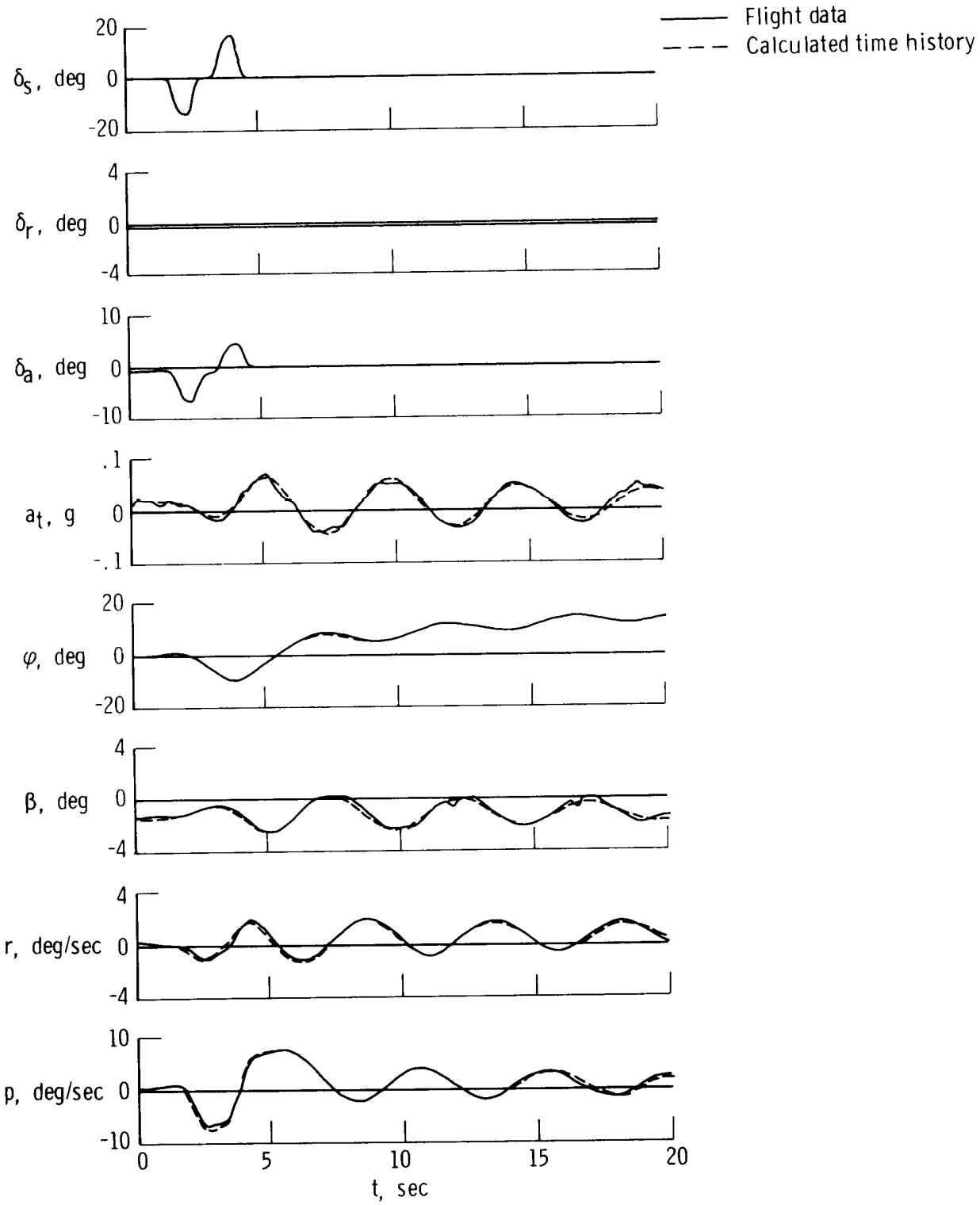

(f) Aileron plus spoiler doublet: M = 0.80, h_p = 10,670 m (35,000 ft), clean configuration.

Figure 6. Concluded.

THIS DOCUMENT PROVIDED BY THE ABBOTT AEROSPACE
TECHNICAL LIBRARY
ABBOTTAEROSPACE.COM

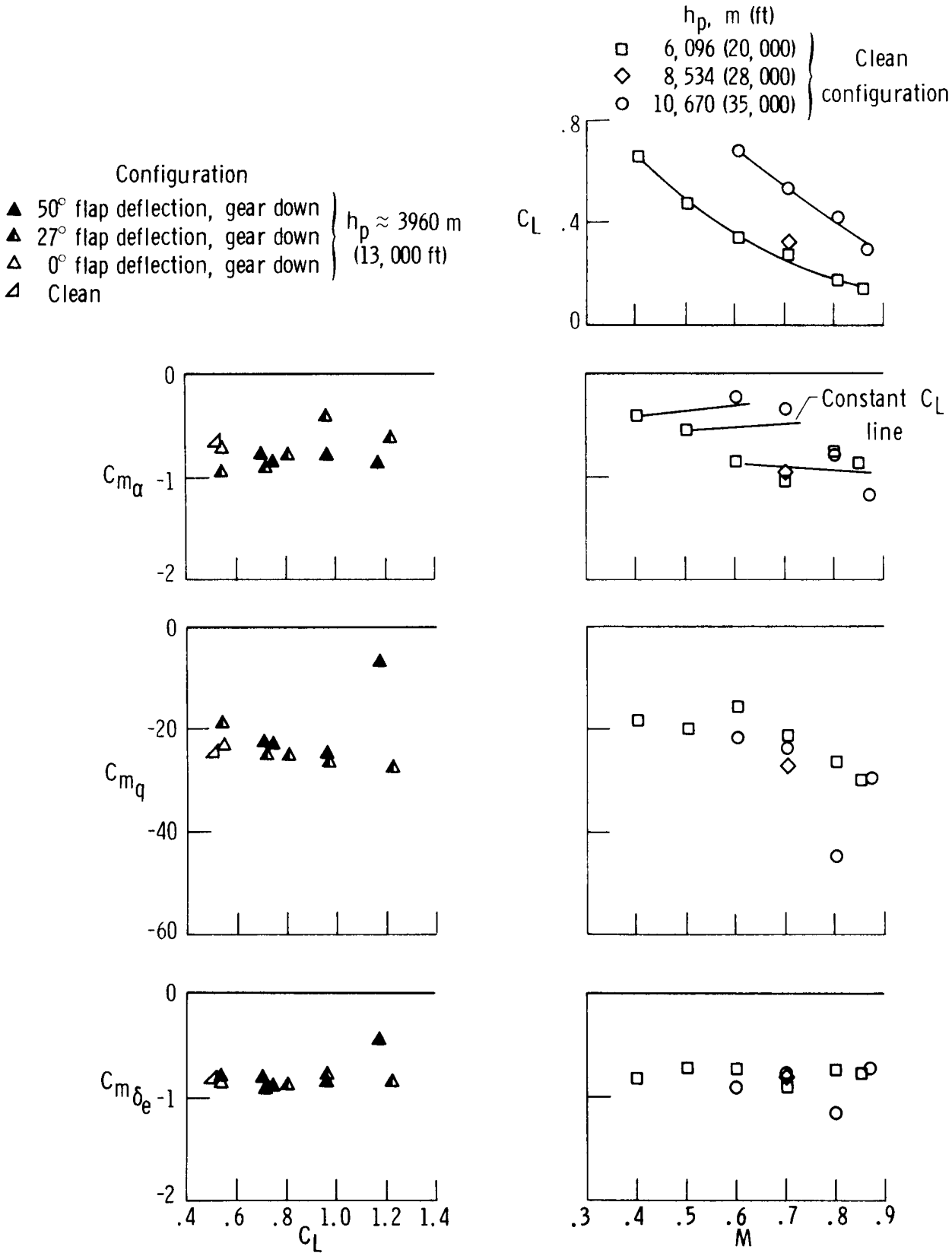

Figure 7. Variation of flight-determined longitudinal pitching-moment derivatives with lift coefficient and Mach number.

THIS DOCUMENT PROVIDED BY THE ABBOTT AEROSPACE
TECHNICAL LIBRARY
ABBOTTAEROSPACE.COM

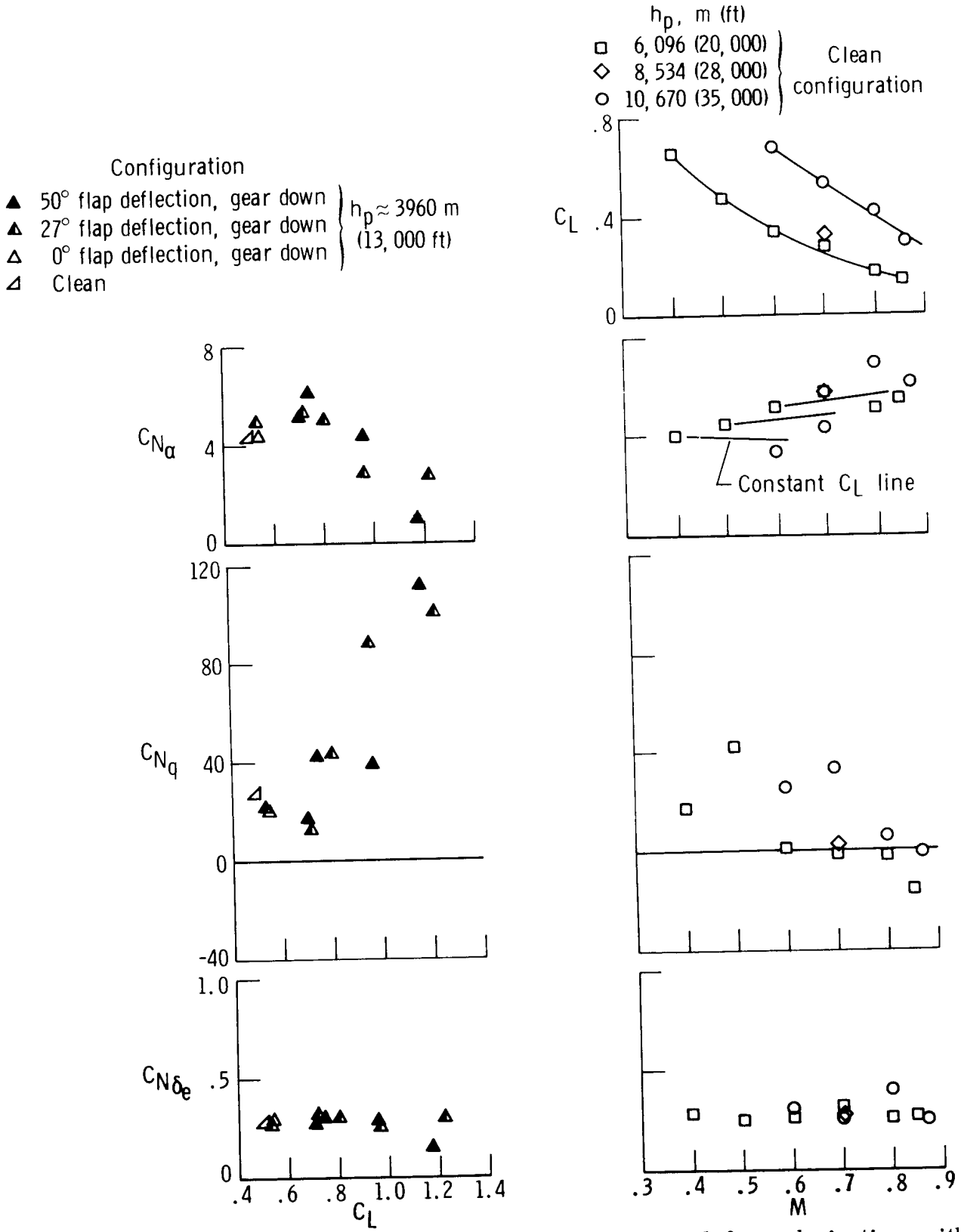

Figure 8. Variation of flight-determined longitudinal normal-force derivatives with lift coefficient and Mach number.

THIS DOCUMENT PROVIDED BY THE ABBOTT AEROSPACE
TECHNICAL LIBRARY
ABBOTTAEROSPACE.COM

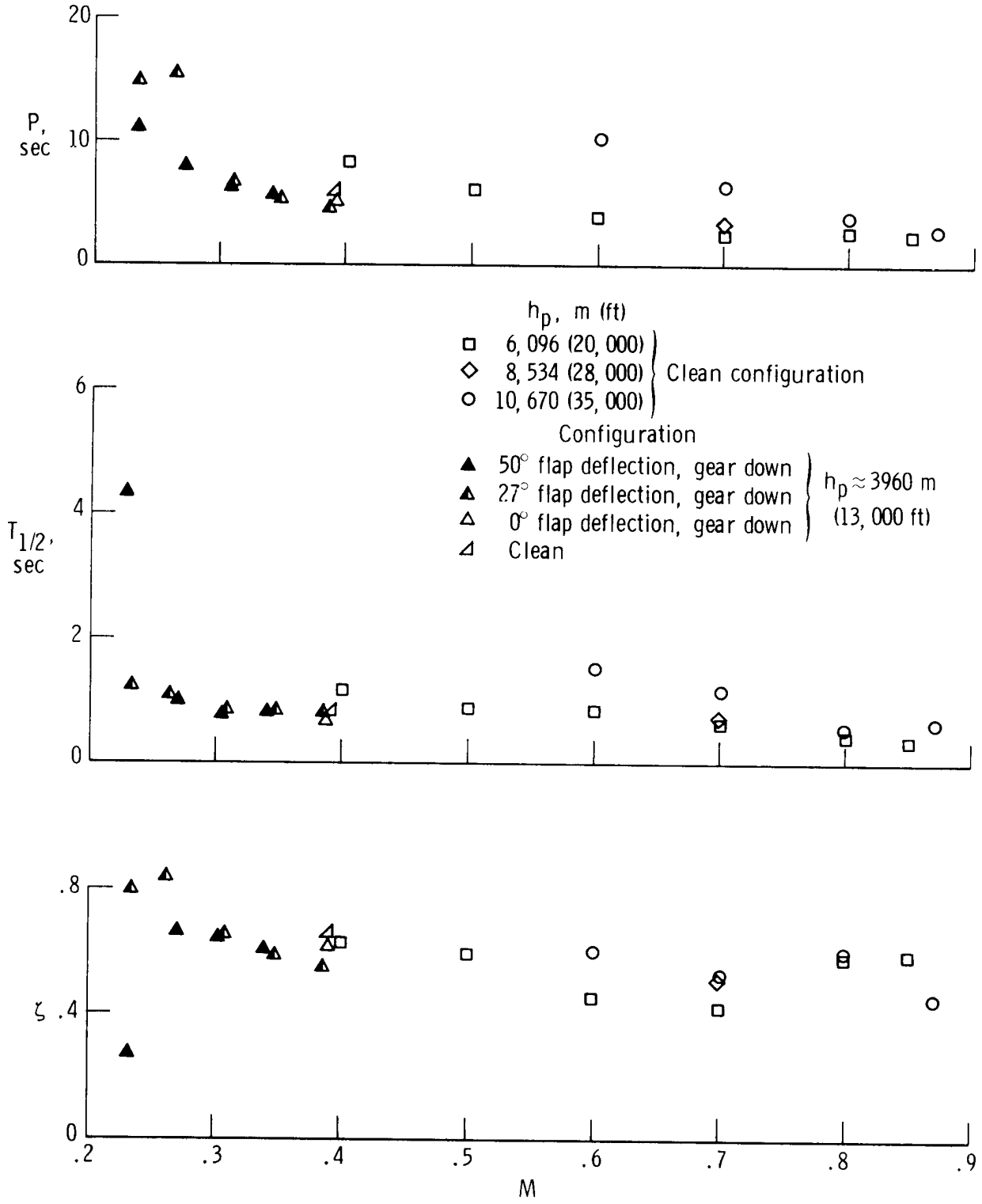

(a) Short-period mode; calculated from flight-determined derivatives.

Figure 9. Variation of longitudinal period and damping characteristics with Mach number.

THIS DOCUMENT PROVIDED BY THE ABBOTT AEROSPACE
TECHNICAL LIBRARY
ABBOTTAEROSPACE.COM

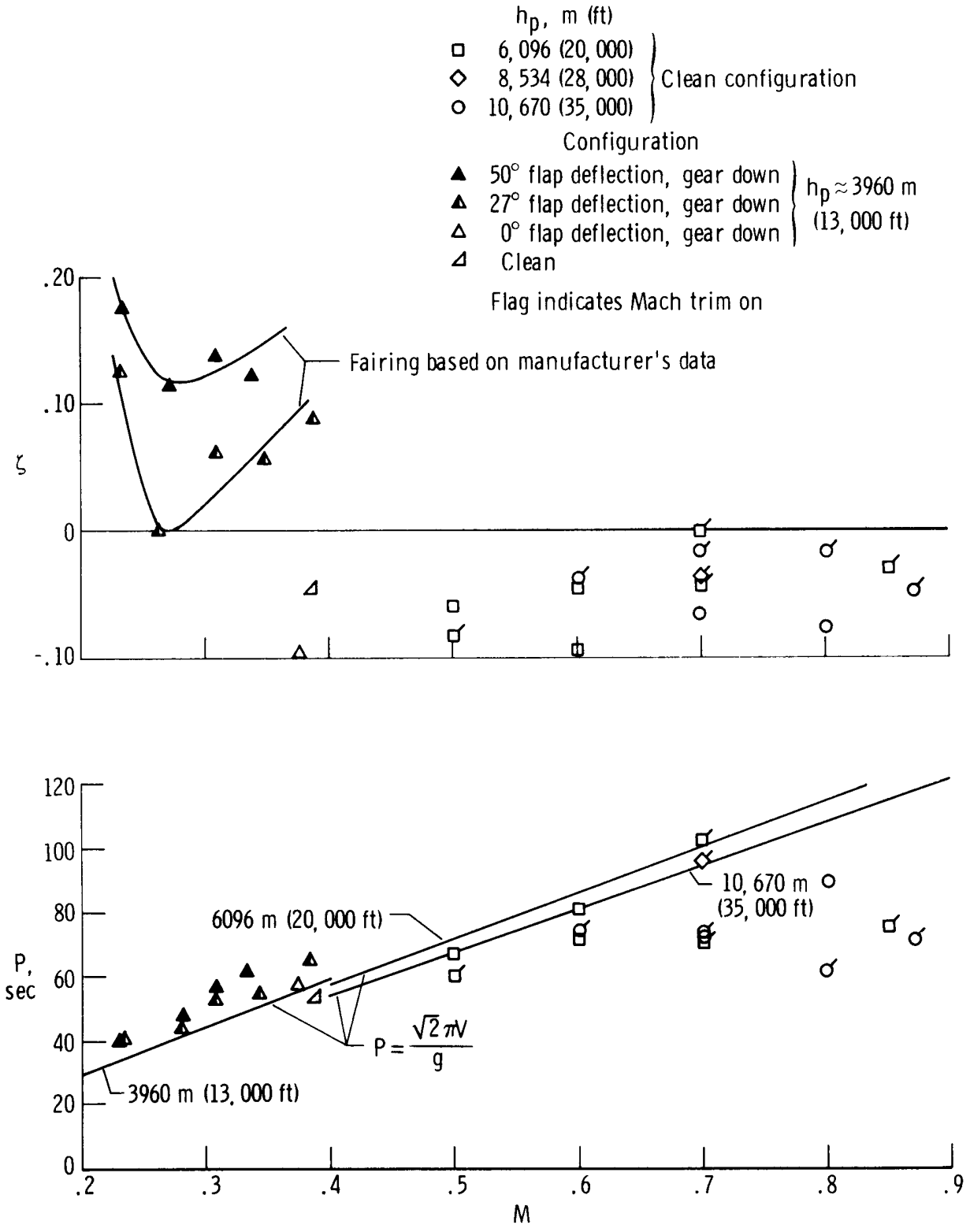

(b) Phugoid mode; measured from flight data.

Figure 9. Concluded.

THIS DOCUMENT PROVIDED BY THE ABBOTT AEROSPACE
TECHNICAL LIBRARY
ABBOTTAEROSPACE.COM

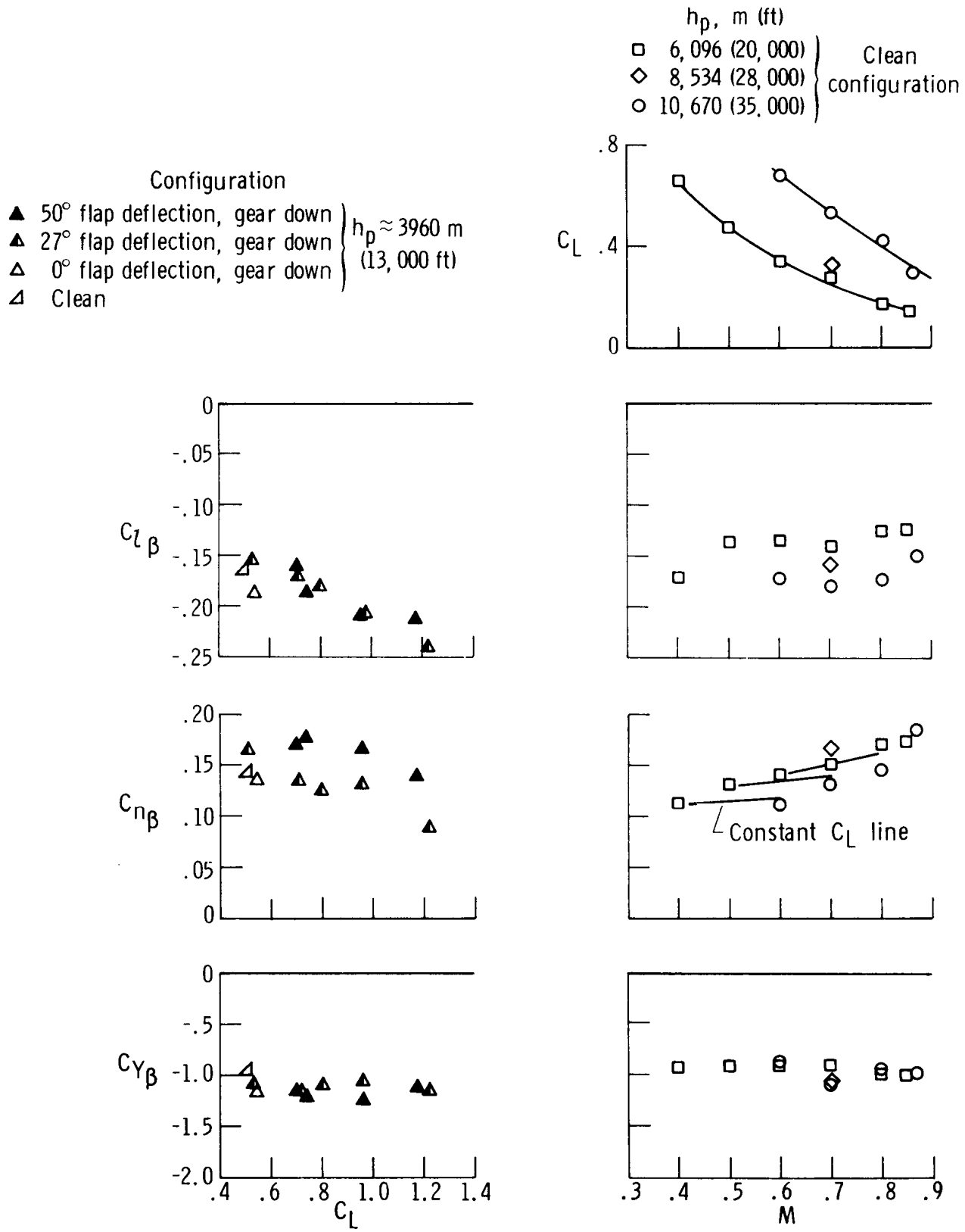

Figure 10. Variation of flight-determined lateral-directional static stability derivatives with lift coefficient and Mach number.

THIS DOCUMENT PROVIDED BY THE ABBOTT AEROSPACE
TECHNICAL LIBRARY
ABBOTTAEROSPACE.COM

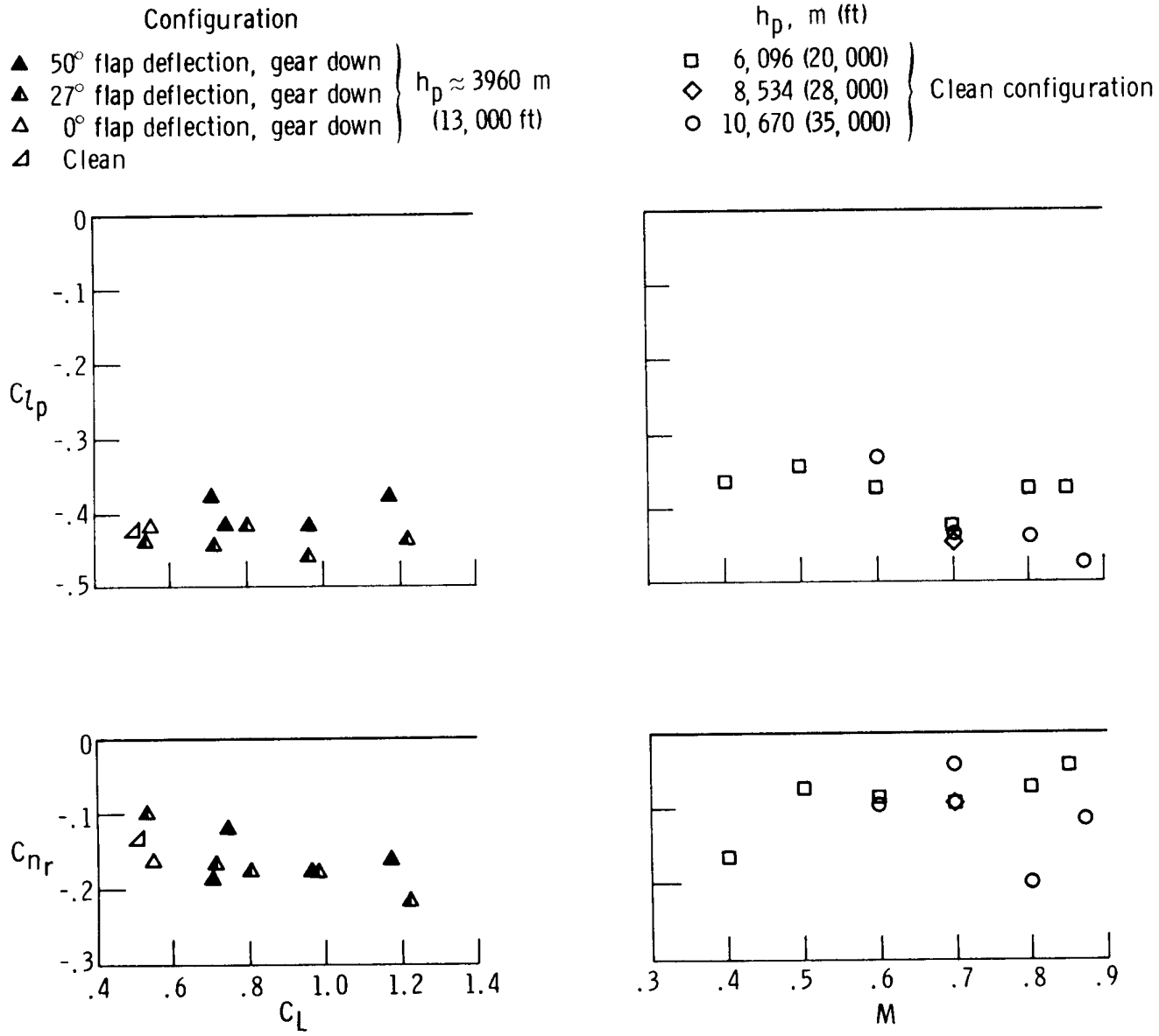

Figure 11. Variation of flight-determined lateral-directional damping derivatives with lift coefficient and Mach number.

THIS DOCUMENT PROVIDED BY THE ABBOTT AEROSPACE
TECHNICAL LIBRARY
ABBOTTAEROSPACE.COM

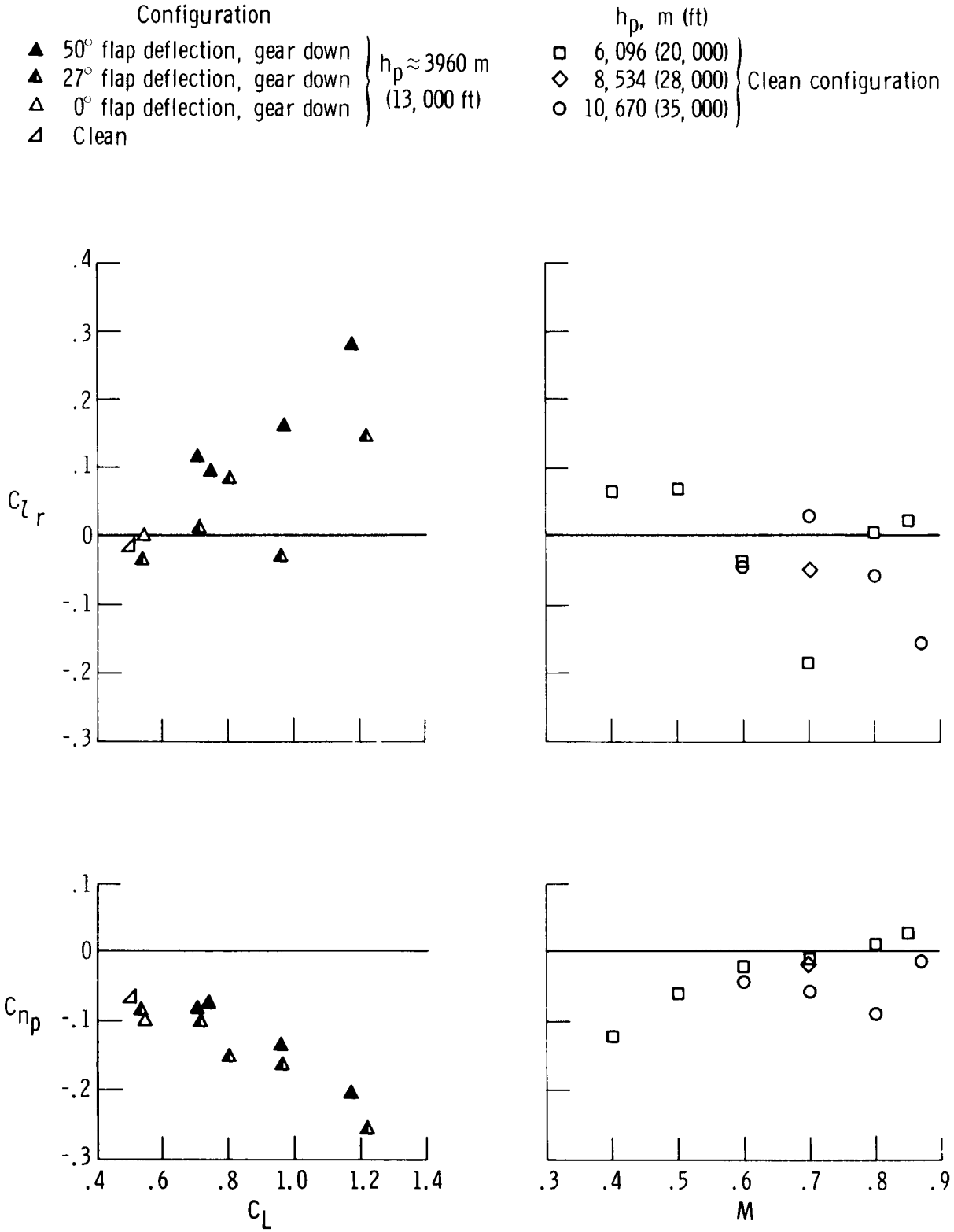

Figure 12. Variation of flight-determined lateral-directional cross-coupling derivatives with lift coefficient and Mach number.

THIS DOCUMENT PROVIDED BY THE ABBOTT AEROSPACE
TECHNICAL LIBRARY
ABBOTTAEROSPACE.COM

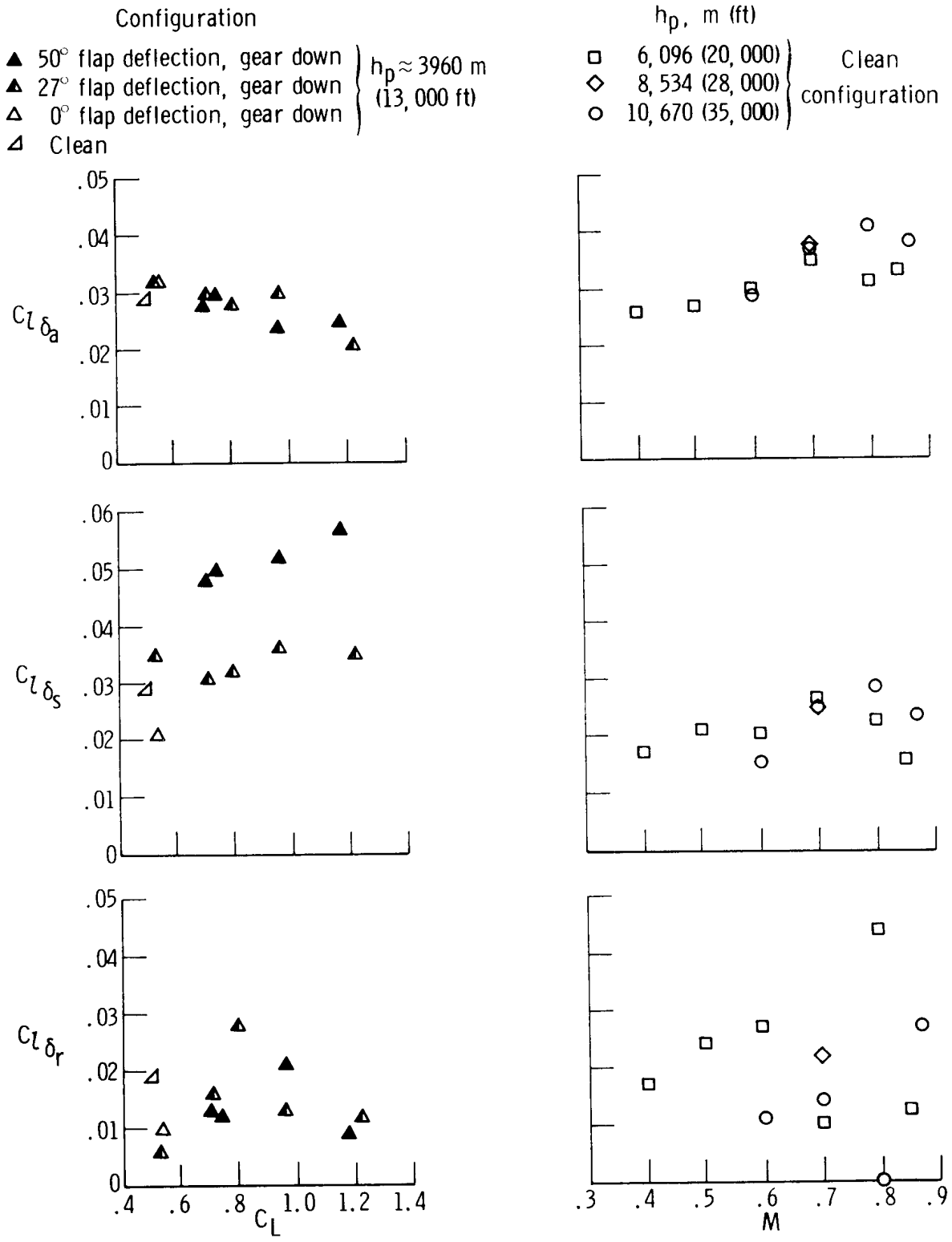

Figure 13. Variation of flight-determined lateral-directional roll control derivatives with lift coefficient and Mach number.

THIS DOCUMENT PROVIDED BY THE ABBOTT AEROSPACE
TECHNICAL LIBRARY
ABBOTTAEROSPACE.COM

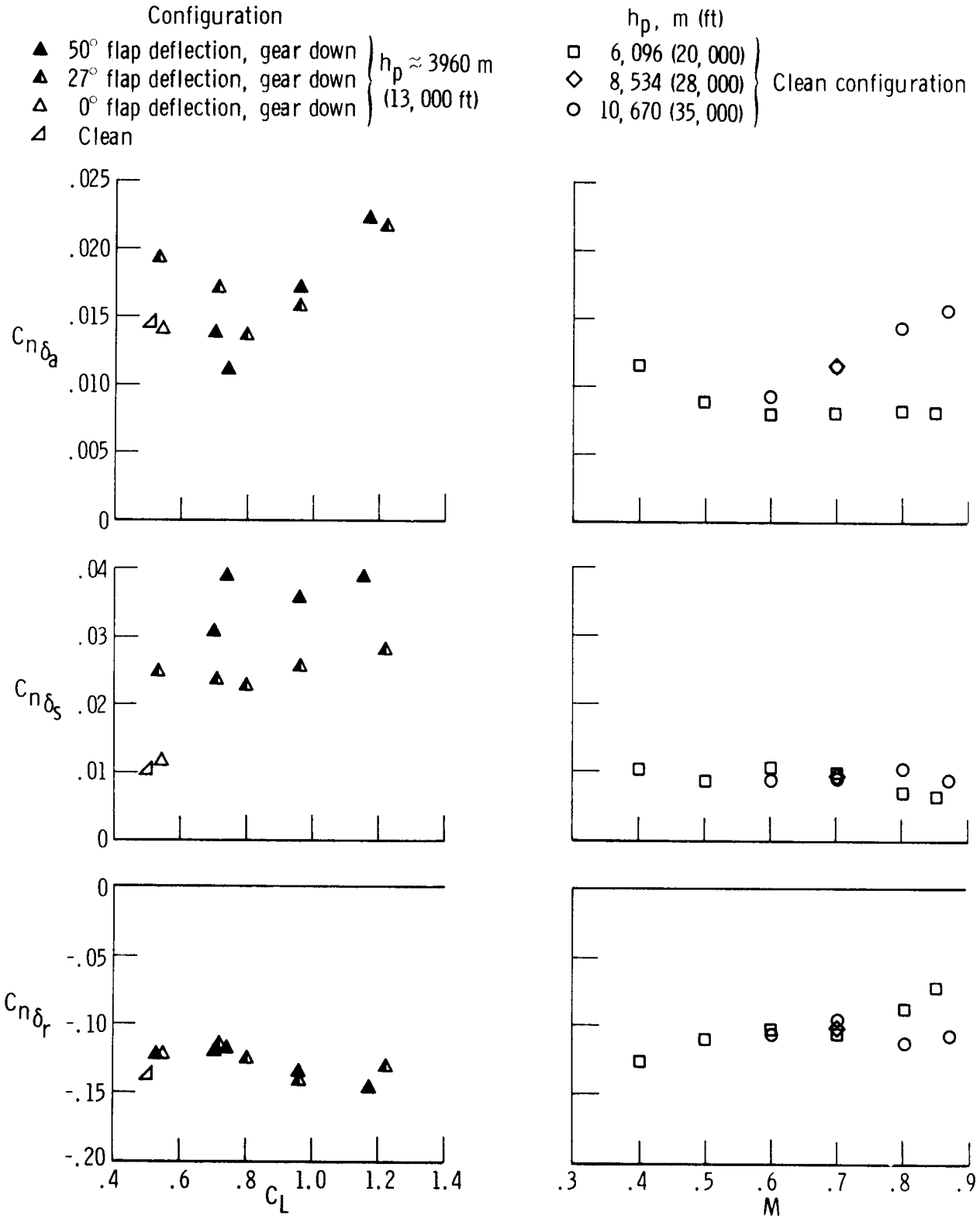

Figure 14. Variation of flight-determined lateral-directional yaw control derivatives with lift coefficient and Mach number.

THIS DOCUMENT PROVIDED BY THE ABBOTT AEROSPACE
TECHNICAL LIBRARY
ABBOTTAEROSPACE.COM

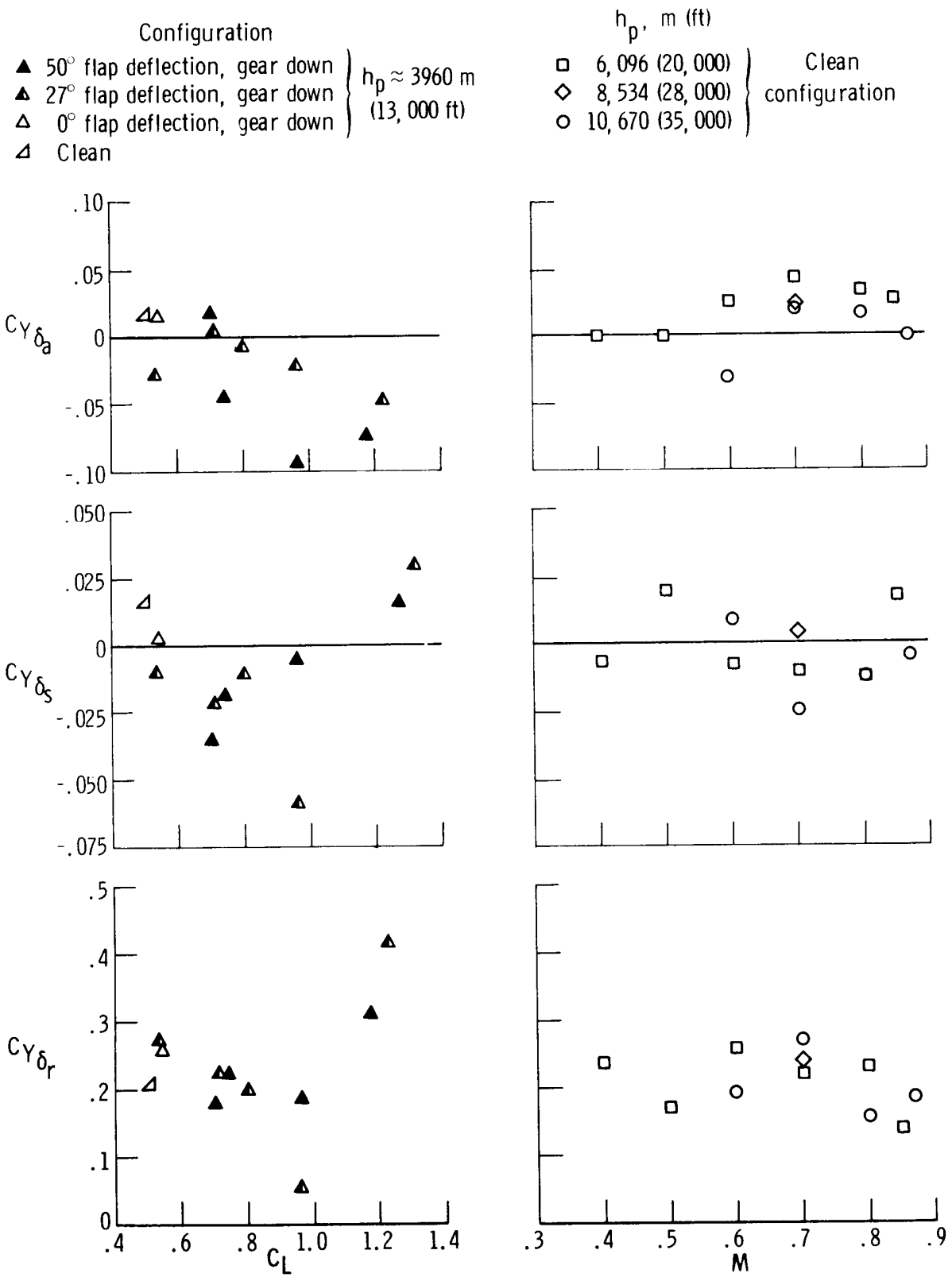

Figure 15. Variation of flight-determined lateral-directional side force control derivatives with lift coefficient and Mach number.

THIS DOCUMENT PROVIDED BY THE ABBOTT AEROSPACE
TECHNICAL LIBRARY
ABBOTTAEROSPACE.COM

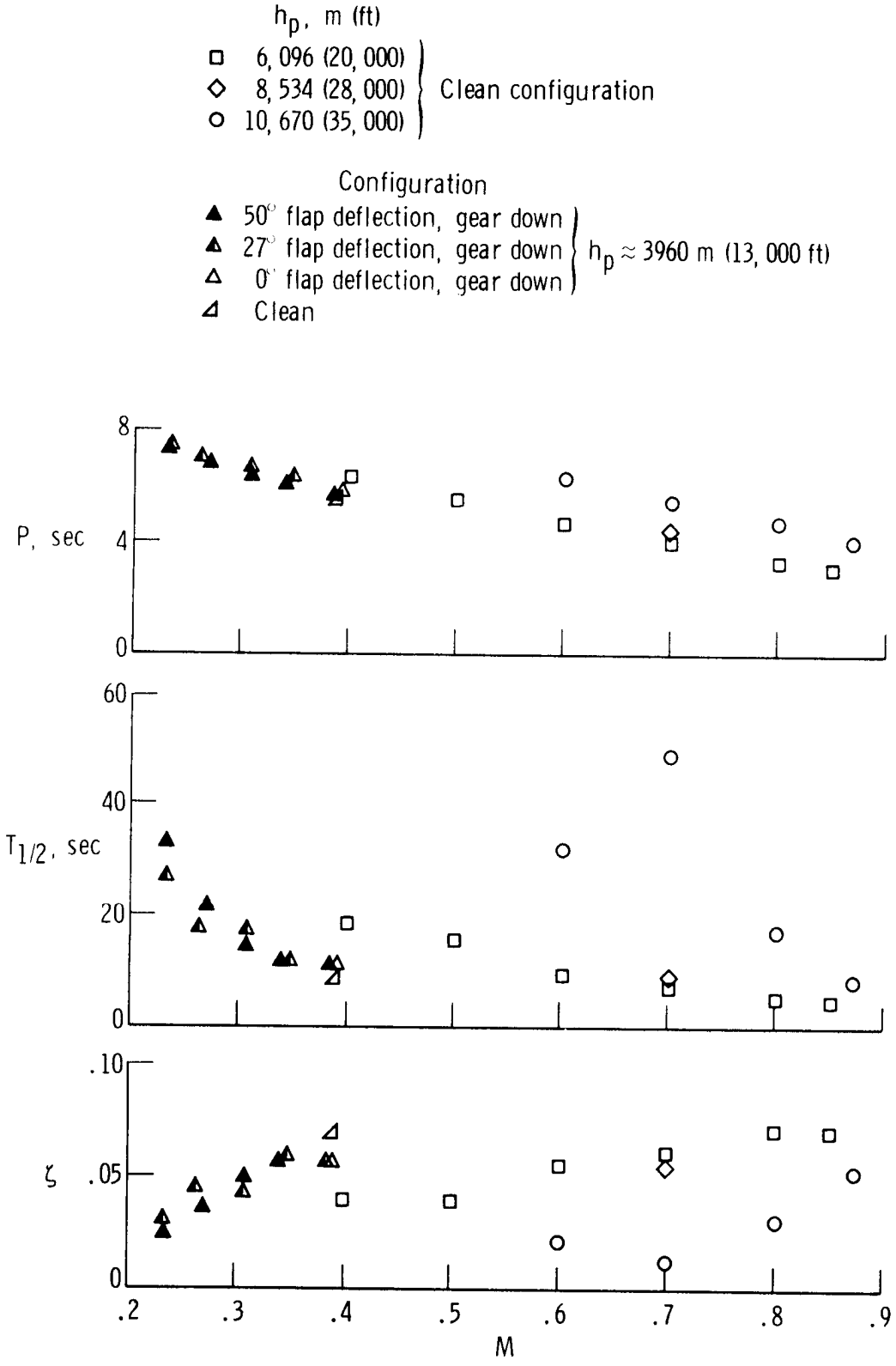

(a) Dutch roll mode period and damping.

Figure 16. Variation of lateral-directional characteristics, calculated from flight-determined derivatives, with Mach number.

THIS DOCUMENT PROVIDED BY THE ABBOTT AEROSPACE
TECHNICAL LIBRARY
ABBOTTAEROSPACE.COM

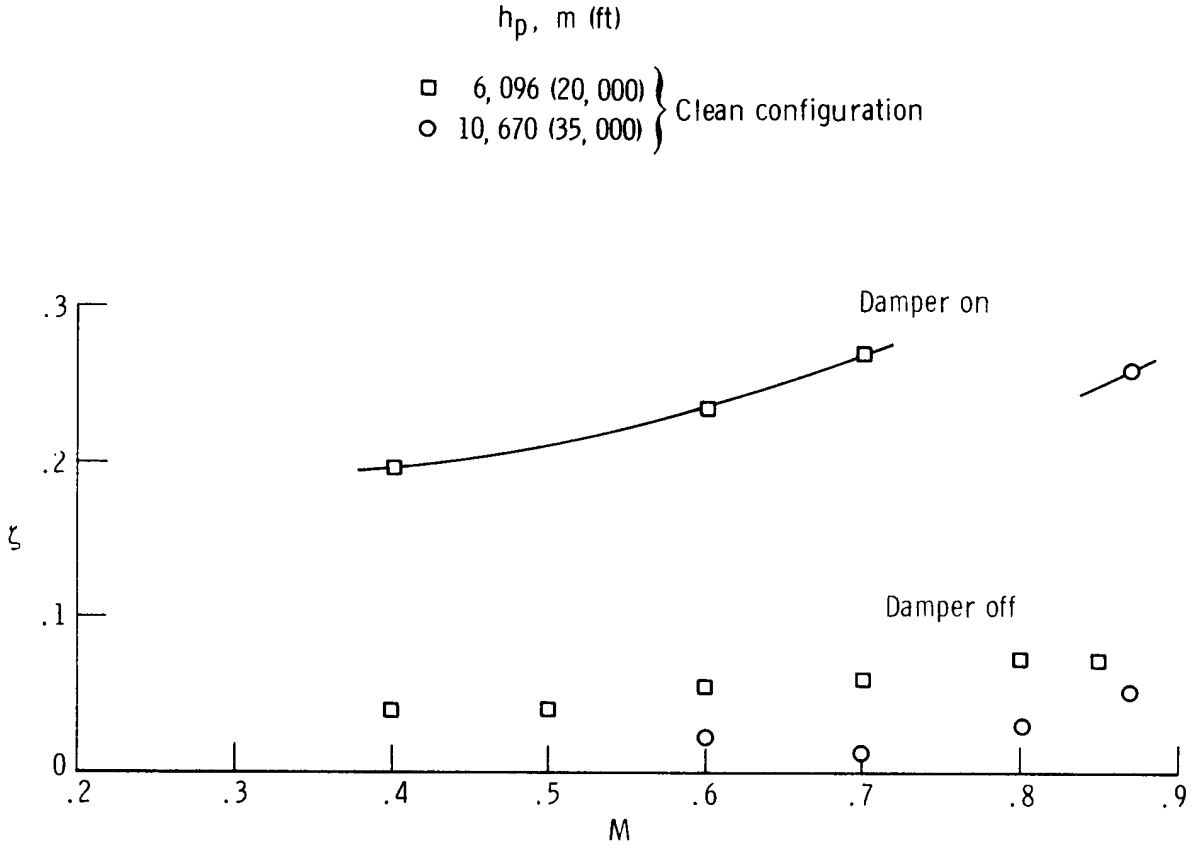

(b) Comparison of damper on and damper off damping ratio.

Figure 16. Continued.

THIS DOCUMENT PROVIDED BY THE ABBOTT AEROSPACE
TECHNICAL LIBRARY
ABBOTTAEROSPACE.COM

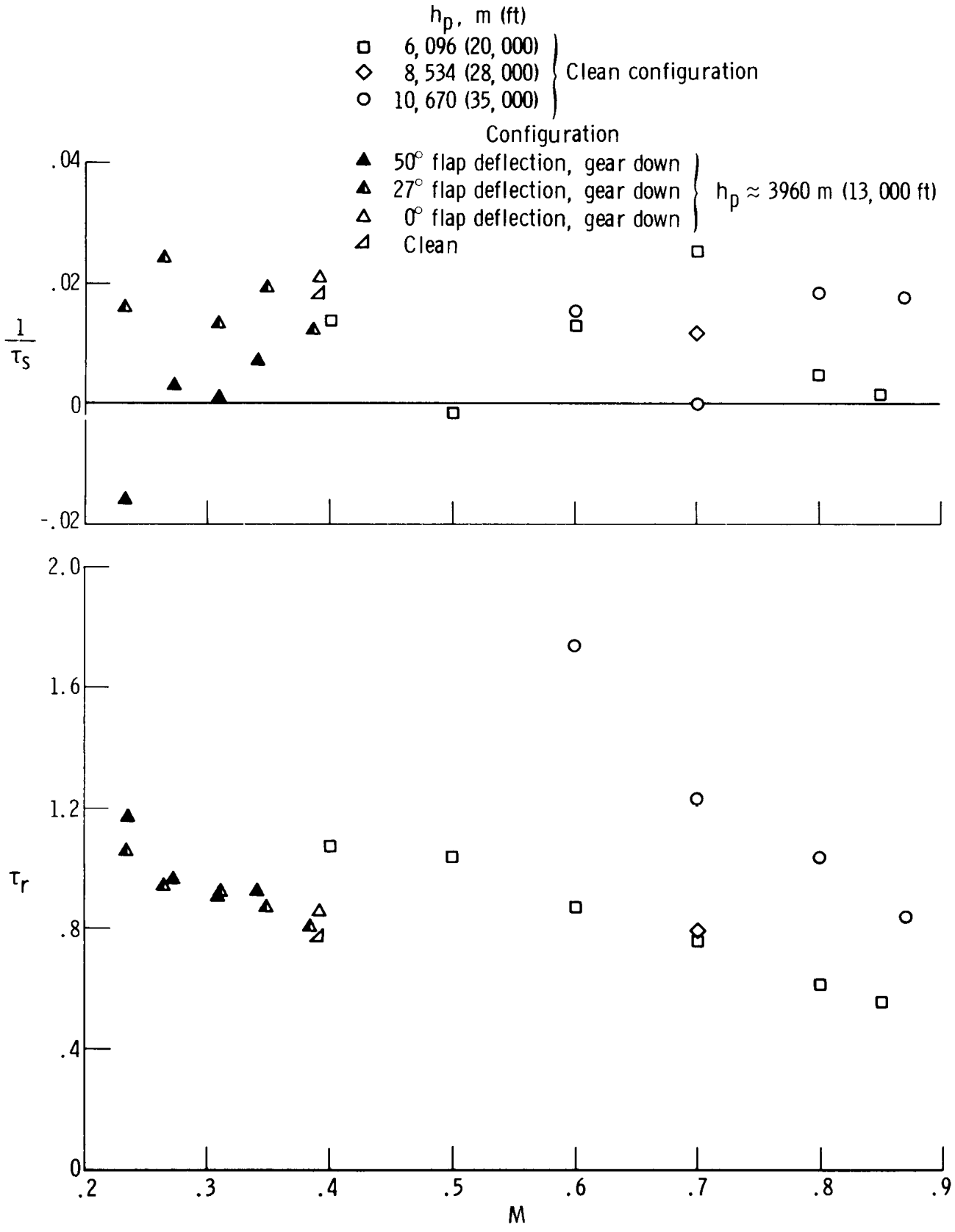

(c) Roll and spiral mode time constants.
Figure 16. Concluded.

THIS DOCUMENT PROVIDED BY THE ABBOTT AEROSPACE
TECHNICAL LIBRARY
ABBOTTAEROSPACE.COM

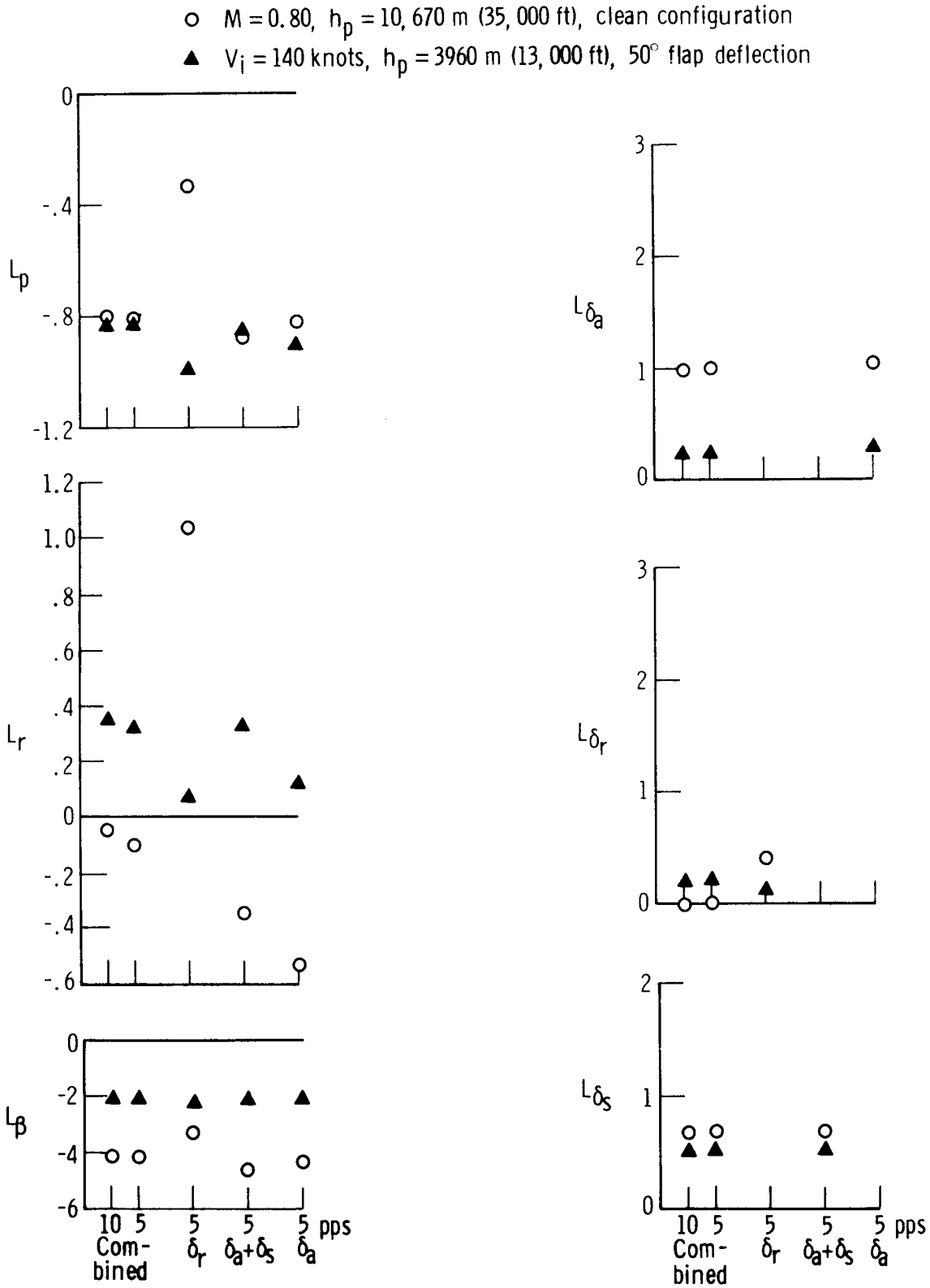

(a) Rolling-moment derivatives.

Figure 17. Comparison of dimensional derivatives obtained by matching maneuvers separately and then simultaneously at a sample rate of 5 points per second (pps) and 10 points per second.

THIS DOCUMENT PROVIDED BY THE ABBOTT AEROSPACE
TECHNICAL LIBRARY
ABBOTTAEROSPACE.COM

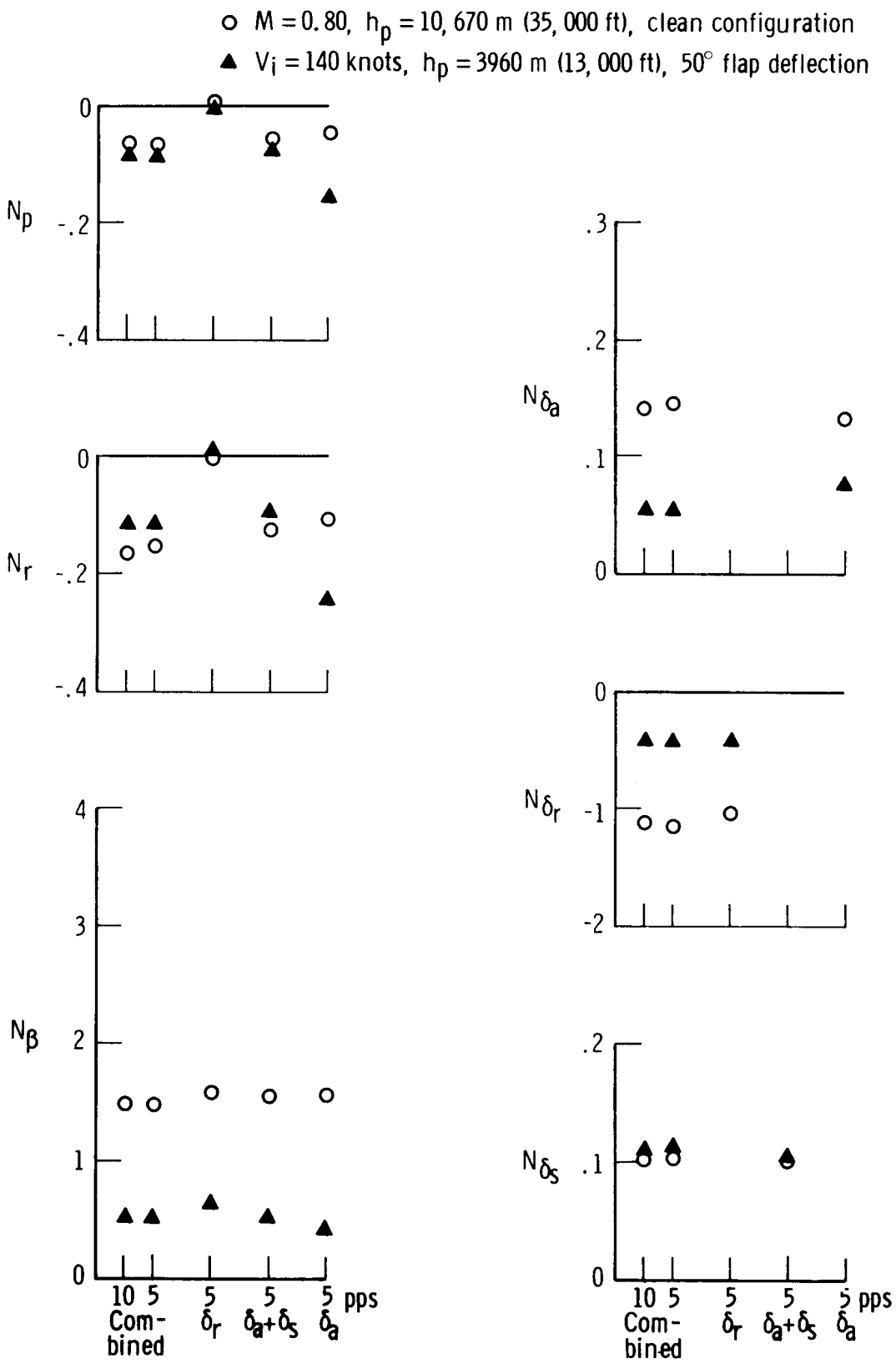

(b) Yawing-moment derivatives.

Figure 17. Continued.

THIS DOCUMENT PROVIDED BY THE ABBOTT AEROSPACE
TECHNICAL LIBRARY
ABBOTTAEROSPACE.COM

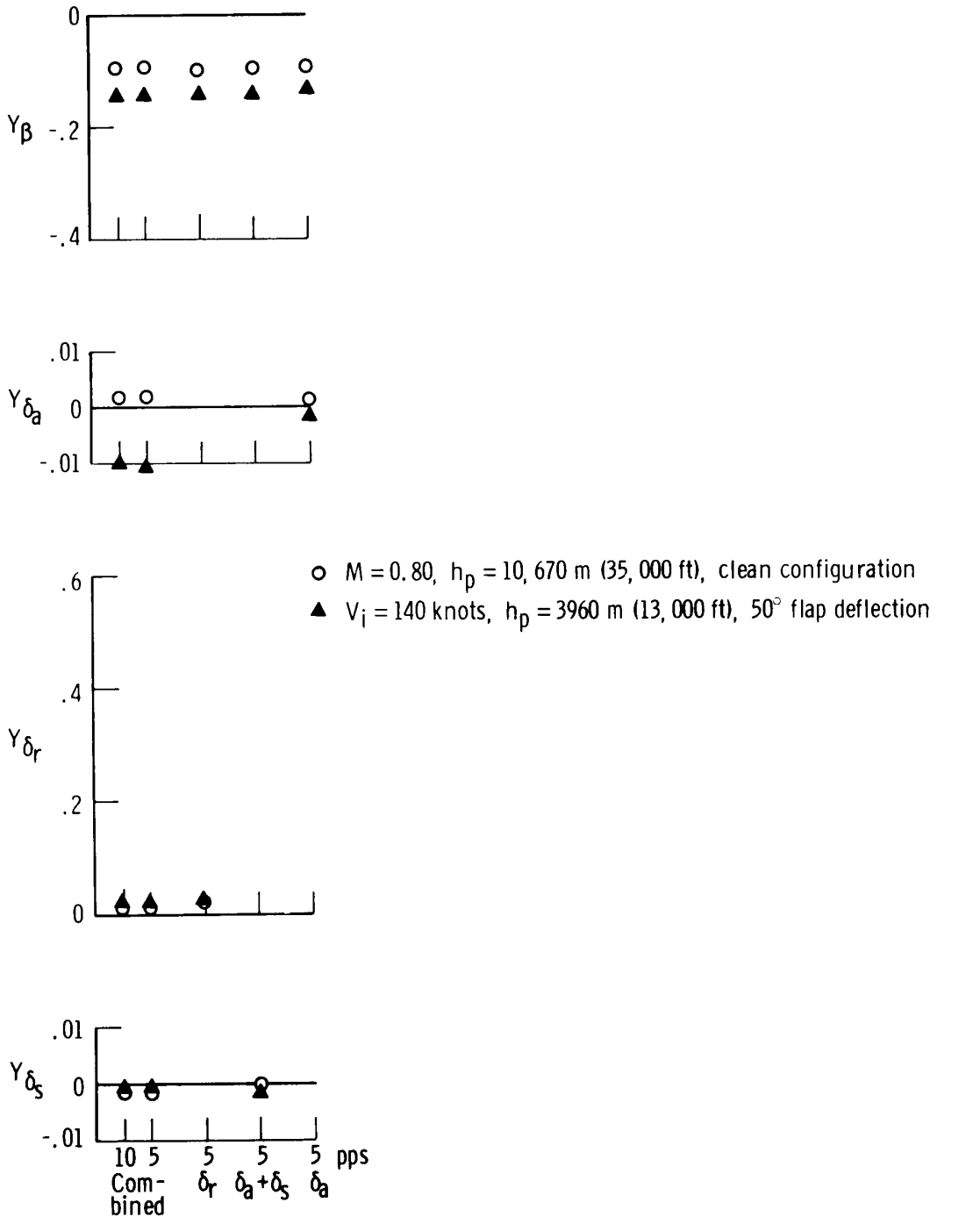

(c) Side force derivatives.

Figure 17. Concluded.

THIS DOCUMENT PROVIDED BY THE ABBOTT AEROSPACE
TECHNICAL LIBRARY
ABBOTTAEROSPACE.COM

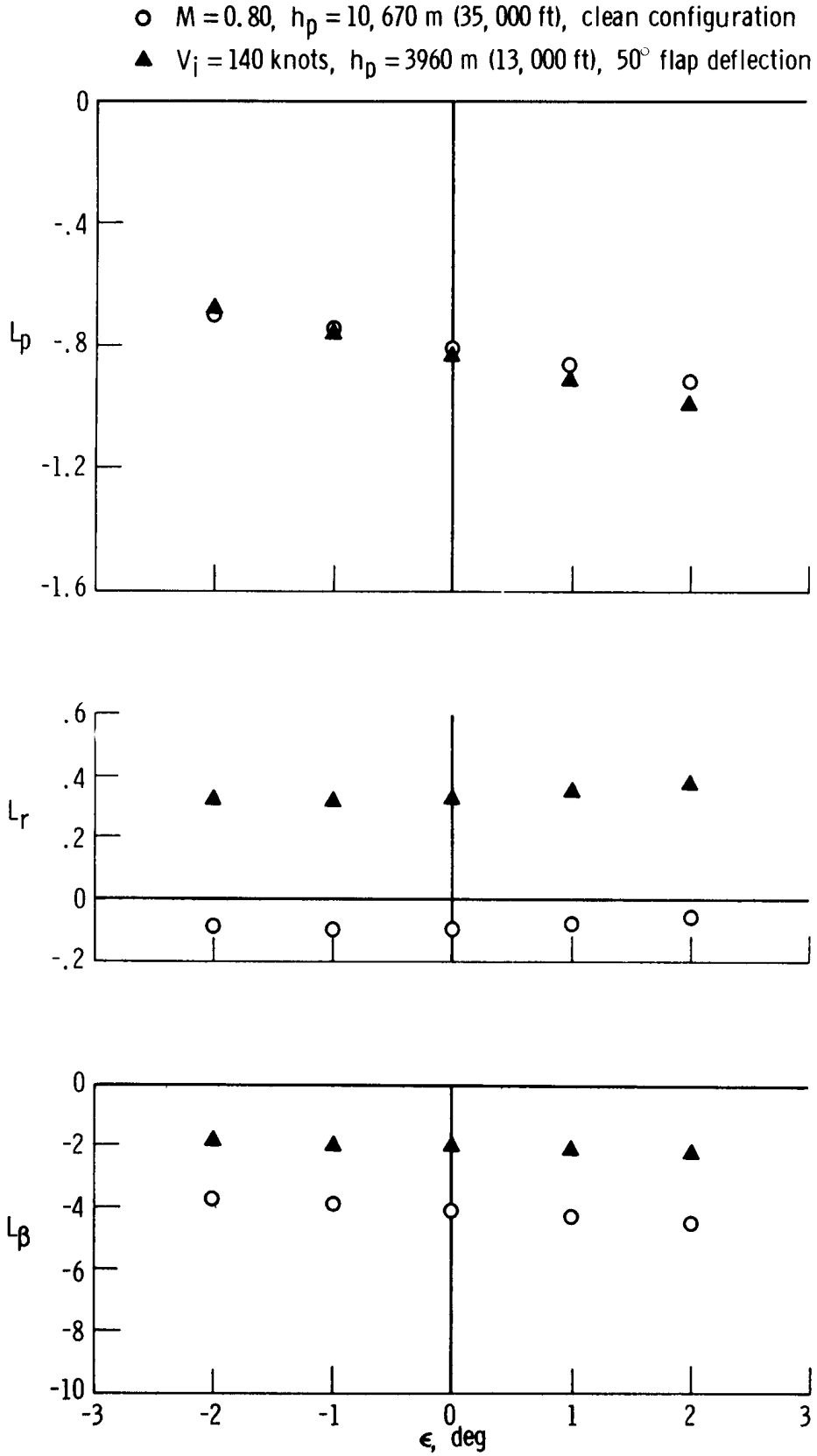

(a) L_p, L_r, L_β.

Figure 18. Variation of dimensional derivatives with principal-axes inclination.

THIS DOCUMENT PROVIDED BY THE ABBOTT AEROSPACE
TECHNICAL LIBRARY
ABBOTTAEROSPACE.COM

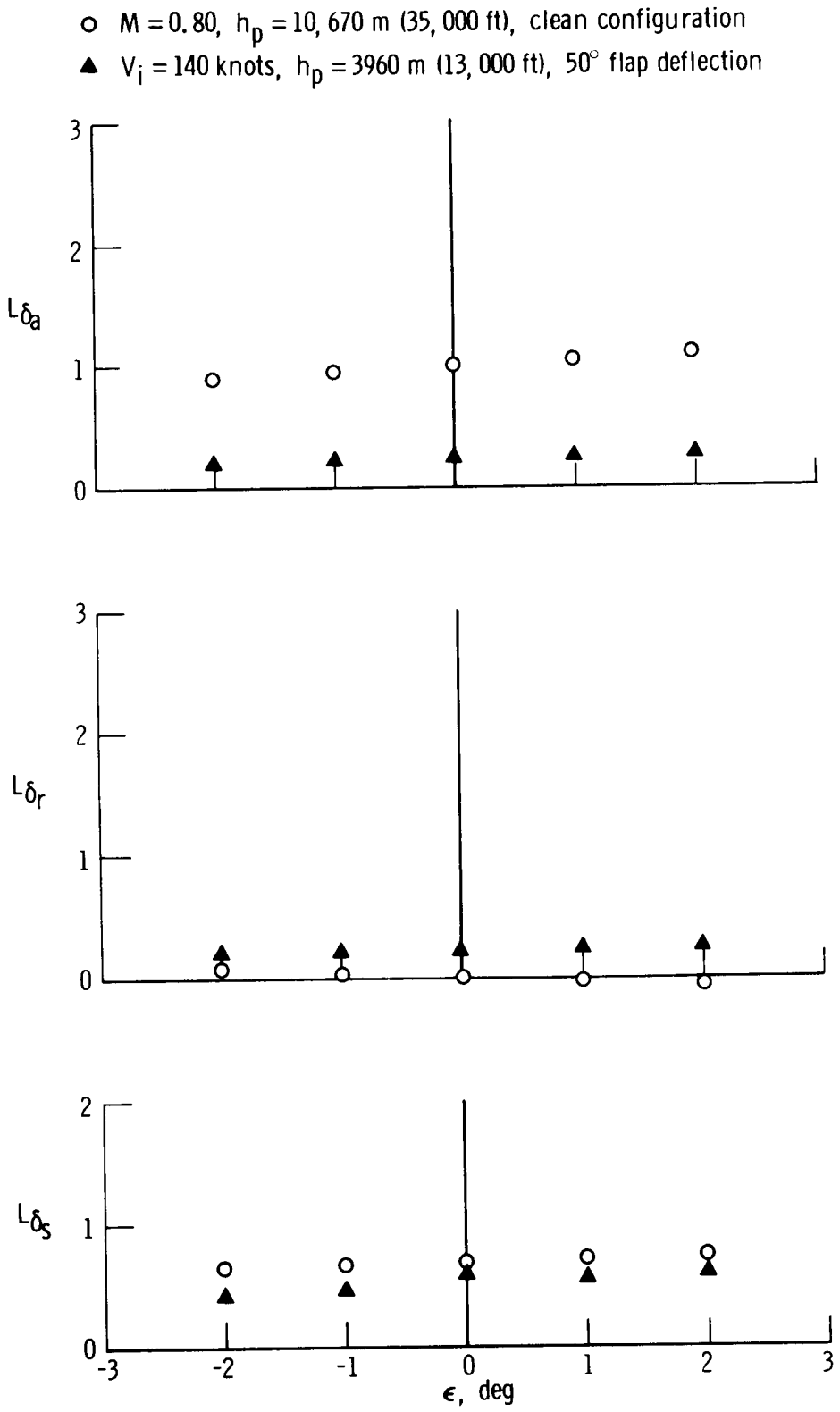

(b) L_{δ_a}, L_{δ_r}, L_{δ_s}.
Figure 18. Continued.

THIS DOCUMENT PROVIDED BY THE ABBOTT AEROSPACE
TECHNICAL LIBRARY
ABBOTTAEROSPACE.COM

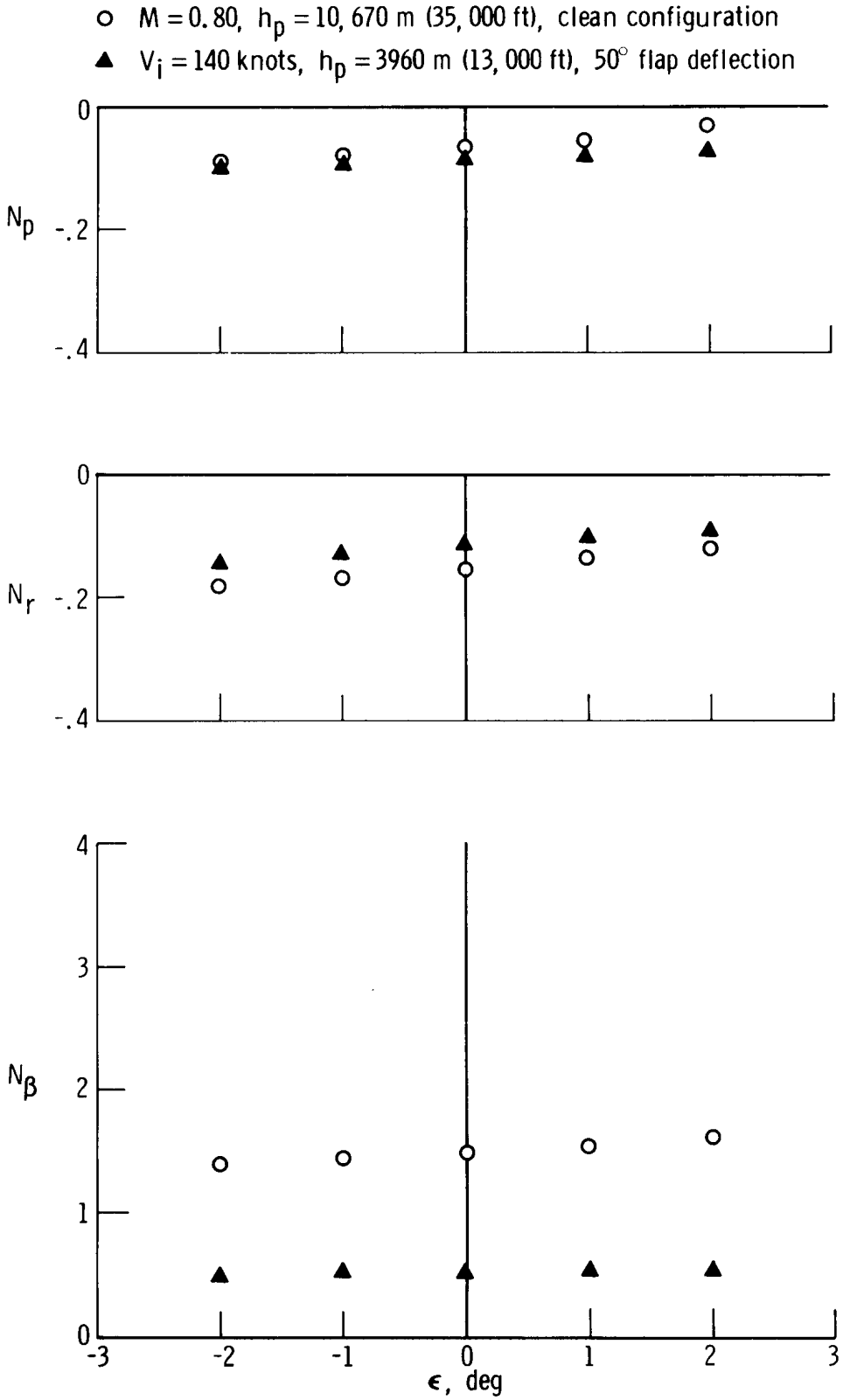

(c) N_p, N_r, N_β.

Figure 18. Continued.

THIS DOCUMENT PROVIDED BY THE ABBOTT AEROSPACE
TECHNICAL LIBRARY
ABBOTTAEROSPACE.COM

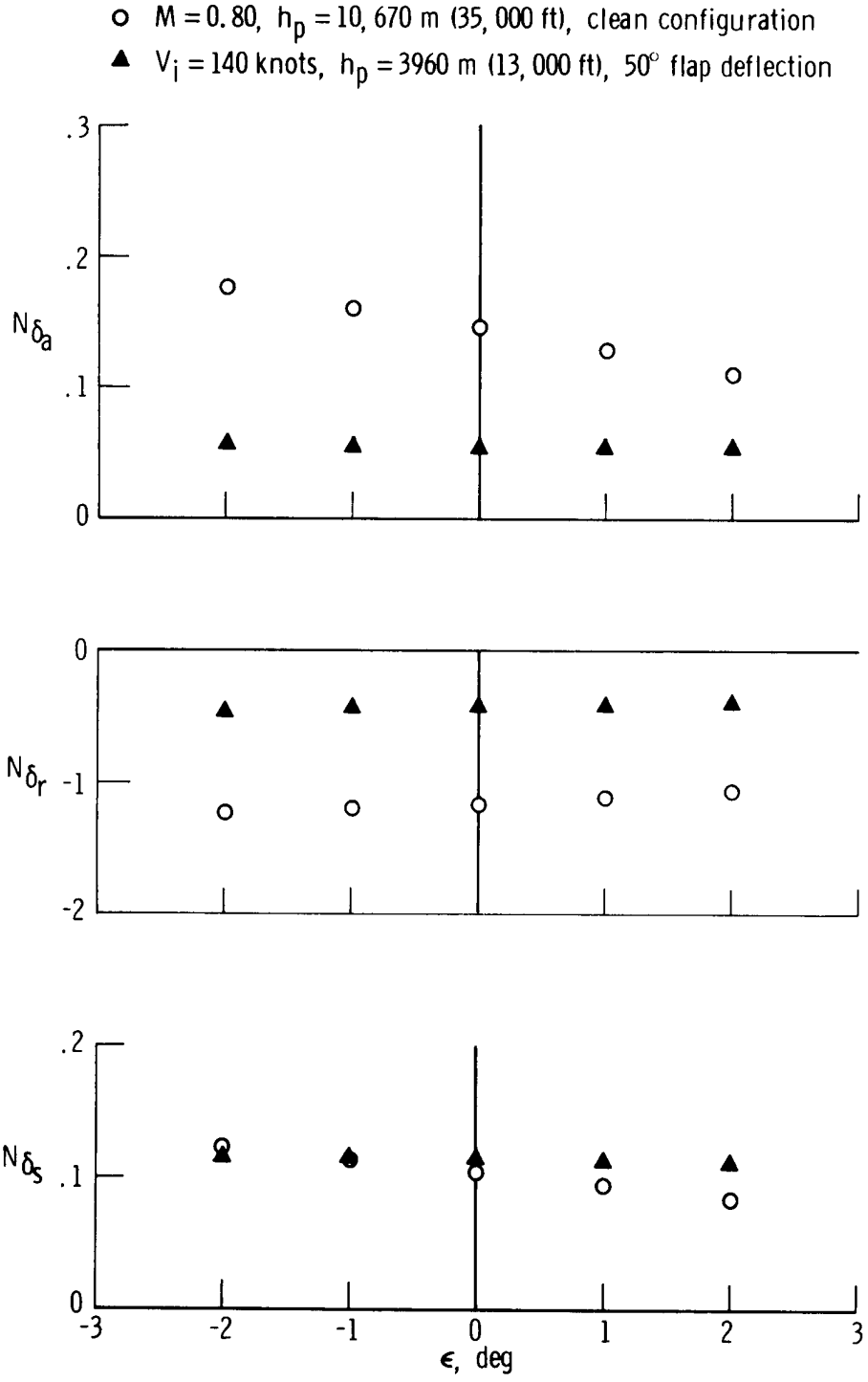

(d) N_{δ_a}, N_{δ_r}, N_{δ_s}.

Figure 18. Continued.

THIS DOCUMENT PROVIDED BY THE ABBOTT AEROSPACE
TECHNICAL LIBRARY
ABBOTTAEROSPACE.COM

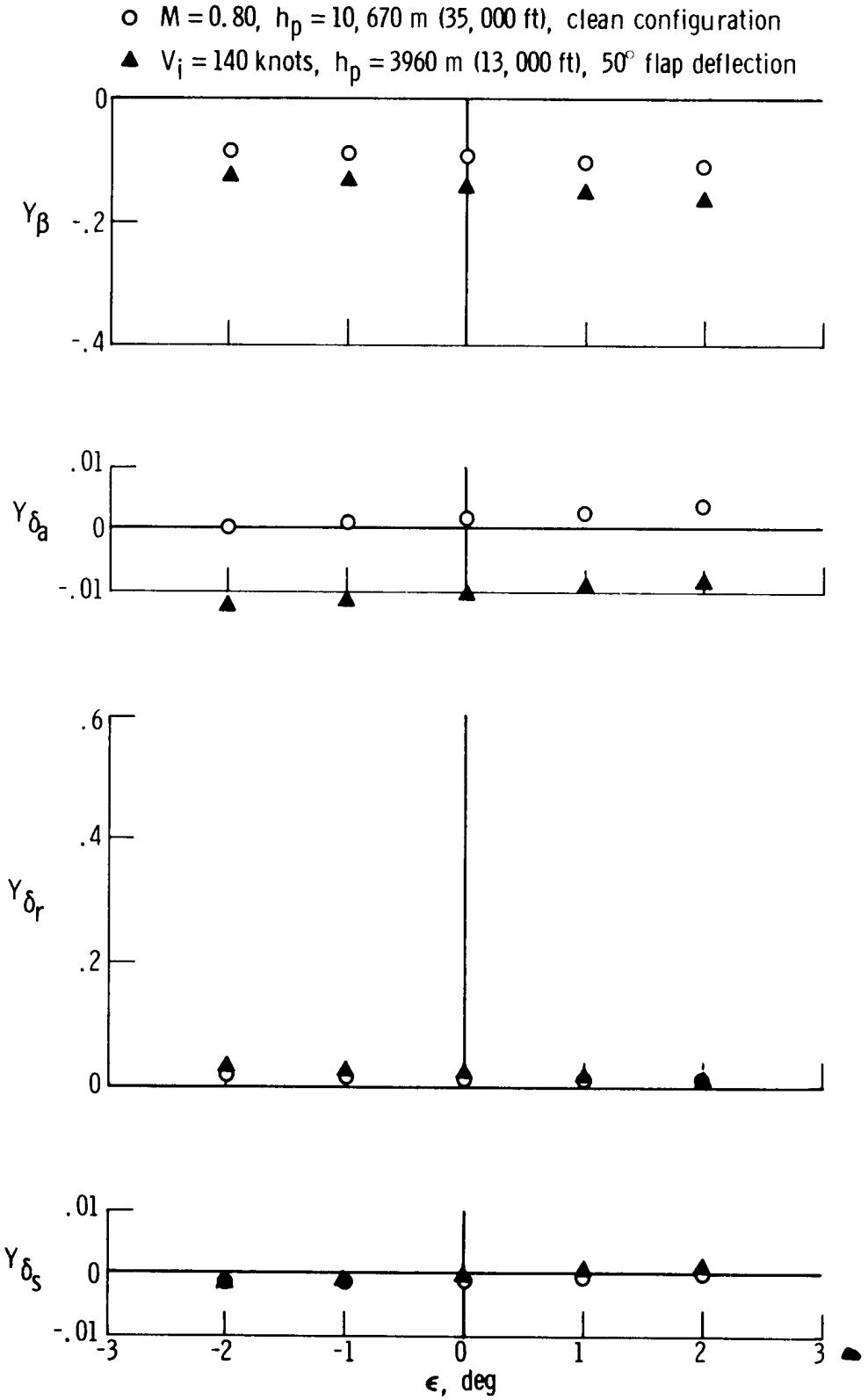

(e) Y_β, Y_{δ_a}, Y_{δ_r}, Y_{δ_s}.

Figure 18. Concluded.

THIS DOCUMENT PROVIDED BY THE ABBOTT AEROSPACE
TECHNICAL LIBRARY
ABBOTTAEROSPACE.COM

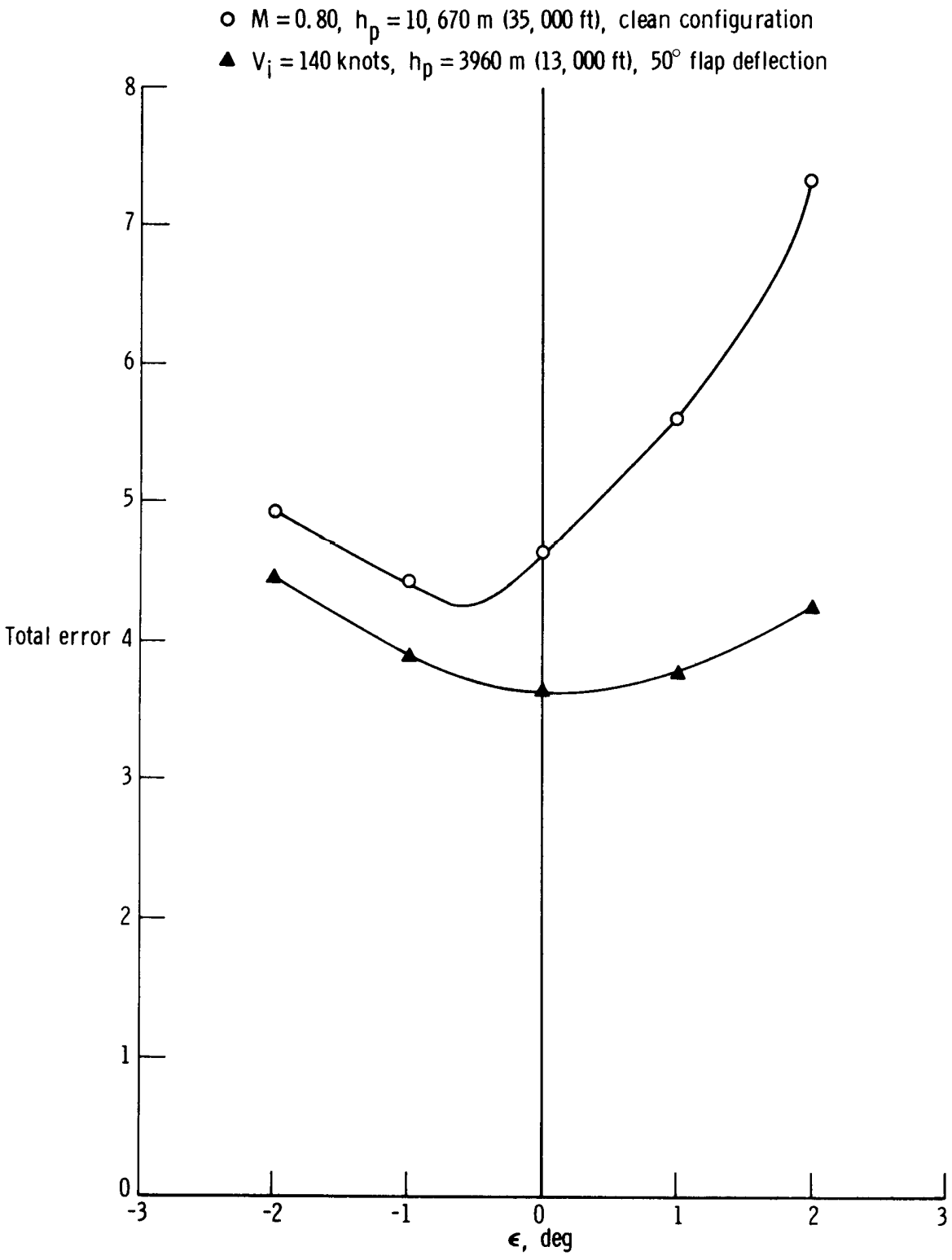

Figure 19. Variation of total error with principal-axes inclination for two flight conditions.